DESY PRC R&D 02/01
The Forward Calorimetry (FCAL) Group
Type of Document: Status Report

R & D for the ILC-Detector: Instrumentation of the Very Forward Region

The Forward Calorimetry Group (FCAL)

VINCA Institute of Nuclear Science, Belgrade, Serbia and Montenegro;
Physics Department, University of Colorado, Boulder, U. S. A.;
Institute of Nuclear Physics, Cracow, Poland;
Faculty of Physics and Applied Computer Sciences, AGH University of Science and Technology, Cracow, Poland;
Joint Institute of Nuclear Research, Dubna, Russia;
Royal Holloway University of London, Great Britain;
NC PHEP, Minsk, Belarus;
Laboratoire de l Accélérateur Linéaire, Orsay, France;
Institute of Physics, Academy of Science, Prague, Czech Republic;
Institute of High Energy Physics, Protvino, Russia;
School of Physics and Astronomy, University of Tel Aviv, Israel;
DESY, Zeuthen, Germany;

April 18, 2006

Contact: Wolfgang Lohmann, wlo@ifh.de

Editors:
H. Abramowicz, K.G. Afanaciev, P. Bambade, V. Drugakov, Ch. Grah, R. Ingbir, E. Kouznetsova, W. Lange, W. Lohmann, K. Mönig, M. Pandurovic, B. Pawlik, C. Rimbault, P. Starovoitov, W. Wierba

See next page for list of authors

Belarus

K. Afanaciev, V. Drugakov, I. Emeliantchik, A. Ignatenko, A. Litomin, N. Shumeiko, A. Solin, P. Starovoitov

NC PHEP, Minsk

Czech Republic

P. Mikes, J. Popule, L. Tomasek, M. Tomasek, V. Vrba

Institute of Physics, Academy of Science, Prague

France

P. Bambade, C. Rimbault

Laboratoire de l Accélérateur Linéaire, Orsay

Germany

Ch. Grah, U. Harder, H. Henschel, E. Kouznetsova, W. Lange, W. Lohmann, K. Mönig, M. Ohlerich, R. Schmidt

Deutsches Elektronensynchrotron Desy, Zeuthen

Great Britain/United Kingdom

G. Blair, J. Carter

Centre for Particle Physics, Royal Holloway University of London

Israel

H. Abramowicz, R. Ingbir, S. Kananov, A. Levy, I. Sadeh, A. Stern

School of Physics & Astronomy, Tel Aviv University

Poland

W. Dabrovski, D. Kisielewska, S. Koperny, J. Lukasik, L. Suszycki, P. Wiacek J. Pieron

Faculty of Physics & Applied Computer Science, AGH University of Science and Technology, Cracow

W. Daniluk, A. Moszczynski, K. Oliwa, B. Pawlik, W. Wierba, L. Zawiejski

Institute of Nuclear Physics, Polish Academy of Sciences, Cracow

Russia

S. Erine, A. Rybine

Institute of High Energy Physics, Protvino

G. Chelkov, A. Elagin, Z. Krumstein, I. Minashvili, A. Olshevski, A. Sapronov

Joint Institute of Nuclear Research, Dubna

Serbia and Montenegro

I. Bozovic-Jelisavcic, J. Mamuzic, M. Pandurovic

VINCA Institute of Nuclear Science, Belgrade

USA

S. Chen, U. Nauenberg, J. Proulx, P. Steinbrecher, J. Zhang

Physics Department, University of Colorado, Boulder

Abstract

Since the last PRC report from the year 2004 the research work of the Forward Calorimetry group (FCAL) has been significantly deepened and extended. The performance of two of the three sub-detectors in the very forward region, LumiCal and BeamCal is investigated for the two interaction regions of the baseline design of the ILC with beam crossing angles of 2 mrad and 20 mrad. In particular, for the larger crossing angle, changes of the forward region compared to the head-on case of the TESLA TDR are necessary. BeamCal and LumiCal must be centered around the outgoing beam-pipe. The BeamCal will have a non-instrumented area to leave space for the second beam-pipe. The inner diameter of LumiCal must be enlarged to avoid substantial depositions from beamstrahlung. New systematic effects of the luminosity measurement, caused by the beam polarization and the bunch charge, are identified. Studies on background from other physics processes are ongoing. More realistic detector simulations, including a more realistic sensor designs and response, show the feasibility of a high precision luminosity measurement. Requirements on the readout electronics are derived from simulations. First exercises with a laser based position monitoring system for LumiCal show that a precision of a few μm can be reached. As an alternative technology for LumiCal, a digital calorimeter is studied.

BeamCal simulations have shown a strong impact of the crossing angle, of the detector magnetic field and of the accelerator parameter settings on the amount and the distribution of the depositions caused by beamstrahlung e^+e^- pairs. For a lattice of different settings these three quantities we have shown that beam diagnostics seems to be feasible with good precision for any design. The performance to detect high energy electrons, however, is different. The latter quantity is of crucial importance for several new particle searches, e.g. sleptons predicted by super-symmetry. An optimization of the detector segmentation is done to reach the highest electron detection efficiency. For diamond sensors, one option to instrument the BeamCal, results are presented on their response as a function of low radiation doses, and on the linearity of the response for large particle fluences.

Conceptional design ideas for the front-end and readout electronics are discussed.

Contents

1 Introduction

The purpose of the FCAL Collaboration is to develop the design for the instrumentation of the very forward region of the future detector at the International Linear Collider (ILC) and to prove the feasibility of detector technologies appropriate for this instrumentation [1]. Presently the following sub-systems are considered, in decreasing order of polar angle: the luminosity detector (LumiCal) for precise measurement of the Bhabha event rate; the beam calorimeter (BeamCal) with the dual purpose of extending the angular coverage of the electromagnetic calorimeter and of providing a fast feed-back in tuning the luminosity; the beamstrahlung photons monitor (PhotoCal) for tuning beam parameters. The latter might be complementary in beam diagnostics to the BeamCal.

The requirement for LumiCal is to enable a measurement of integrated luminosity with a relative precision of 10^{-4}. Two possible designs are considered, both based on a tungsten/silicon sandwich calorimeter with a typical angular coverage of 26 to 92 mrad. They differ in the sensor structure. In the first version all sensor planes are subdivided into pads and in the second, the sensor planes are alternating layers of strips and rings. The use of Bhabha scattering as the gauge process is motivated by the fact that the cross-section is large and dominated by electromagnetic processes and thus the cross section can be calculated with very high precision.

The purpose of the BeamCal is to efficiently detect high energy electrons and photons produced e.g. in low transverse momentum QED processes such as Bhabha scattering and photon-photon events. The latter is important in order to suppress this dominant background in many searches for new particles predicted in scenarios for physics beyond the Standard Model. In the polar angle range covered by the BeamCal, typically 5 to 27 mrad, high energy electrons must be detected on top of a large flux of low energy e^+e^- pairs originating from beamstrahlung photon conversions. The measurement of the total energy deposited by these pairs, bunch by bunch, can be used to monitor the variation in luminosity and can provide a fast feedback to the beam delivery system. Moreover, the analysis of the shape of the energy flow can be used to extract the parameters of the colliding beams. This information can be further used to optimize the machine operation.

PhotoCal can be used to analyze beamstrahlung photons emitted at relatively large angles. It will be positioned at a distance of few hundred meters from the interaction point (IP), covering polar angles of the order of a few 100 μrad. It will be sensitive to the tail of the beamstrahlung photon distribution, which in turn is sensitive to the beam parameters.

For the presented studies, these sub-detectors are embedded within the Large Detector Concept (LDC) [2], which is a successor of the detector presented in the TESLA-TDR [3]. The layout is presented in Figure 1[1] [4]. The location of the LumiCal and BeamCal is of critical importance for the background in the main detector. BeamCal acts as a mask in front of the final quadrupole magnets reducing backscattering from pairs. The aperture of LumiCal is such that only a small amount of photons backscattered from the BeamCal reaches the inner detector while it is large enough to let pass the pairs from beamstrahlung.

[1]The most recent design of LDC very forward region differs from the one shown here. The changes were only recently agreed upon, and most of the results presented do not depend on the details of the design.

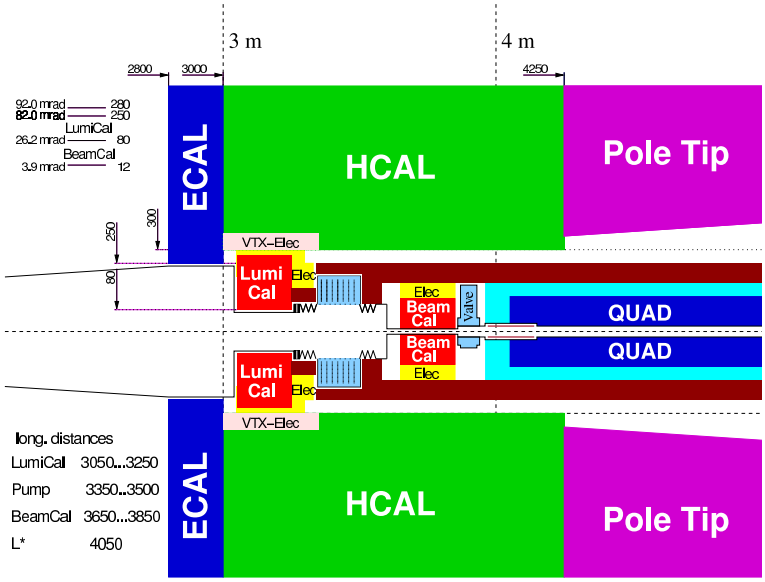

Figure 1: The layout of the forward region of the LDC detector, as considered in the presented studies. The angular coverage of LumiCal and BeamCal, as well as the distance from the IP are given in the figure.

Note that for different beam crossing angles and different magnetic field configurations, the energy distributions of the pairs changes and the amount of backscattered particles might be considerably different. The latter has implications on the optimal location of the very forward calorimeters and their polar angle coverage.

In the following, we report on the progress made since the last PRC, one and a half year ago. The importance of the forward calorimeters for the physics potential of the ILC detector is briefly covered. The impact of beam polarization and other physics processes on the luminosity measurement is considered. The optimization of the design of LumiCal and BeamCal based on simulations is described for several beam crossing angle and accelerator operation schemes. Results on sensor tests are given, followed by a discussion of a concept of electronic readout scheme for both detectors. At the end we confront the status of the research work with the previously set milestones and describe our future plans.

2 Physics Case for the Forward Instrumentation

2.1 Precision Luminosity Measurement

To measure the cross-section, σ, of a certain process we count the events, N, registered in the detector, and obtain the cross section using the corresponding integrated luminosity, $\mathcal{L}$, $\sigma = N/\mathcal{L}$. Neglecting other systematic uncertainties, the required precision on the luminosity measurement is given by the statistics of the highest cross-section processes we want to measure. At $\sqrt{s} = 340$ GeV the cross-section of $e^+e^- \to W^+W^-$ is about 10 pb and the one of $e^+e^- \to f\bar{f}$ is about 5 pb, both scaling with $1/s$. In both processes one thus expects event samples of $\mathcal{O}(10^6)$ events in a few years of running, which would require a luminosity precision of $\Delta\mathcal{L}/\mathcal{L}$ of better than 10^{-3}.

W-pair production is given by neutrino t-channel exchange and Z or γ s-channel exchange. The t-channel part is strongly peaked in the forward region and dominates the total cross-section. If the $We\nu$ coupling is taken from the Standard Model, all information on anomalous gauge couplings can thus be obtained from a fit to the W angular distribution (combined with some decay angles) so that no luminosity measurement is needed. However, if there is a reason to remeasure the $We\nu$ coupling at the ILC a precise luminosity determination is necessary.

The situation is completely different for fermion pair production. For $f \neq e$, only the interesting s-channel diagrams are present and the normalization has to be taken from an external luminosity measurement. As an example Figure 2 shows the expected exclusion limits on Z' bosons obtained from the two-fermion cross sections for different assumptions on the systematic uncertainties [5]. For the η model, only the cross-section error is important while for the other models the errors on the luminosity and the polarization are relevant. Similar requirements hold for the search for contact interactions or other indirect signatures for physics beyond the Standard Model.

In the GigaZ mode more than 10^9 hadronic Z decays are expected which would in principle require a luminosity precision around 10^{-5}. However there are other systematic uncertainties, like the selection efficiency for hadronic events and the modification of the cross-section on top of the Breit-Wigner resonance due, to the beam energy spread, that seem hard to get under control at this level. Hence a luminosity precision of $\Delta\mathcal{L}/\mathcal{L} \sim 10^{-4}$ seems sufficient. The goal of the GigaZ run is a test of the radiative corrections to the Z-fermion couplings with extremely high precision. In general these radiative corrections can be parametrized in terms of three parameters, e.g. $\varepsilon_{1,2,3}$ [6]. Figure 3 shows the expected precision on $\varepsilon_{1,3}$ under different assumptions [7]. These two parameters can be obtained from the Z-observables alone while ε_2 needs in addition a measurement of the W-mass. The narrow axis of the ellipse is given by the measurement of the effective weak mixing angle which is obtained from asymmetry measurements, and does not require an absolute luminosity measurement. For a limit on the Higgs boson mass, within the Standard Model, this measurement is sufficient. In most extensions of the Standard Model, ε_1 and ε_3 can vary in a wide range while ε_2 stays at its Standard Model value. The large axis of the ellipse can be constrained by a precise measurement of the W-mass, so that also in this case no absolute luminosity measurement is required. In the most general case, where also

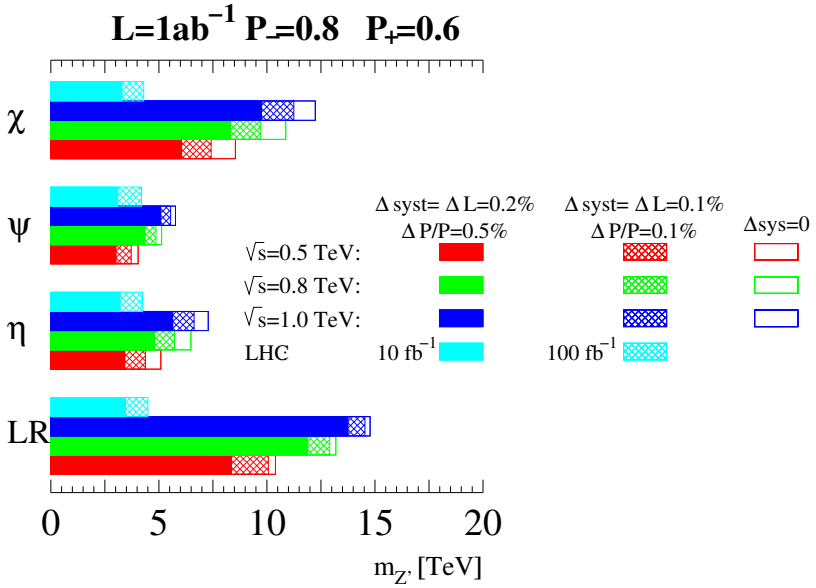

Figure 2: Sensitivity to different Z' models estimated for the ILC for several centre-of-mass energies, as denoted in the figure, and for the LHC

ε_2 is allowed to deviate from its Standard Model value, the large axis is determined by the partial widths of the Z for which cross-section measurements are an essential input.

GigaZ is especially interesting when no direct evidence for physics beyond the Standard Model is found. In this case the structure of radiative corrections should be tested without artificial constraints so that the high precision on the luminosity is definitely required.

2.2 Physics Searches

The forward calorimeters are an important tool to identify two photon events by detecting either one electron or positron with an energy near to the beam energy. Two photon events constitute the most serious background for many search channels which are characterized by missing energy and missing momentum. Lets consider e.g. the search for the slepton and neutralino particles with quasi-degenerate masses which are predicted in some interesting realizations of the super-symmetric model. It has been shown, in the context of the co-annihilation scenario, that staus and neutralinos could combine to provide a plausible, quantitative, explanation for the amount of dark matter in the universe [8]. In the phenomenological analysis which was carried out, the framework of super-gravity was used for definiteness in the predictions. Given constraints from recent WMAP measurements, such scenarios appeare to be favoured.

It is assumed that the sleptons are the heavier particles. They are pair-produced and then decay into the lighter neutralinos, which escape undetected, and regular leptons. If the masses are very close, the produced leptons are soft, with a momentum range which can be directly related to the difference of masses between the slepton and neutralino.

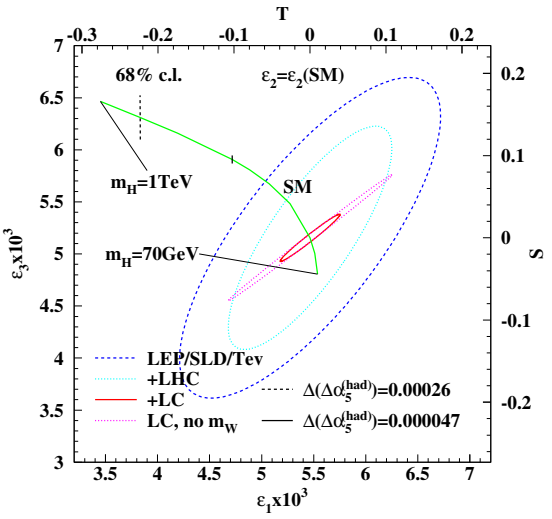

Figure 3: Precision for $\varepsilon_{1,3}$ present, and expected after the LHC and after the ILC measurements. All curves, apart from the one denoted "LC, no m_W", assume that ε_2 is equal to its SM value which is true in most, but not all, extensions of the Standard Model.

Since the relative orientation of the slepton decays is arbitrary, the two leptons are usually very acoplanar. In most cases, lepton pairs produced in photon-photon processes have a significant different topology and kinematics and can be rejected by simple cuts. However, since the two photon cross-section is typically five orders of magnitudes larger, events in the tails of the kinematic distributions become important. The most dangerous events occur in the tail of the spectator electron transverse momentum distribution. When the spectator electron is in the acceptance of the BeamCal, the produced lepton pair can be acoplanar enough to look like the searched signal events. Such events must be vetoed by explicit detection of the spectator electron in the BeamCal. The range of angles where such a veto is needed can be estimated from simple kinematic arguments in relation to the slepton-neutralino mass difference. For a 5 GeV mass difference, rejection is needed down to 10 mrad in the case of smuons and down to roughly 5 mrad for staus. The requirement is more stringent for staus because of the additional loss of energy and momentum due to the neutrinos in the tau lepton decay. The level of rejection required has been estimated in [9] for the case of a stau search analysis optimized for a 5 GeV mass difference. It was found that for a good part of the BeamCal acceptance, after taking into account the rejection from other analysis cuts, involving for instance the topology and kinematics of the events, spectator electron suppression factors ranging between 10^{-1} and 5×10^{-4} were needed in the BeamCal, when going from the innermost part of the acceptance (at about 4 mrad) towards its largest values. With such rejection factors, signal to background values of order one could be achieved. This requirement was estimated for the particular benchmark scenario in [8]. It should be taken as indicative and will in general depend on the

exact mass difference and cross-sections involved.

To obtain such values, a very good separation must be achieved between high-energy electrons with momenta close to that of the beam and the pile-up of low-energy beamstrahlung pairs. The most difficult region is the innermost part of the acceptance, where most of the beamstrahlung pairs are stopped. Our studies have shown that an electron veto inefficiency between 10^{-3} and 10^{-4} could be achieved in most of the BeamCal area, beyond the innermost ring. It has also been shown that for geometries involving a large crossing-angle, the distortion in the beamstrahlung pair profile in the BeamCal, from the transverse components of the solenoidal field, can seriously reduce the capability to veto high-energy electrons. ILC beam parameter sets where the luminosity is achieved with increased beamstrahlung, e.g. the Low Power and High Luminosity sets [10], are also less favourable in this respect.

Another aspect of the requirement comes from the need to avoid excessive veto due to Bhabha scattering events superimposed on signal events. The probability for this to occur is not negligible in the lower part of the acceptance. To minimize the impact, Bhabha events must be identified in the BeamCal with good efficiency, by exploiting as much as possible the coincidence, back-to-back topology and energy balance with both sides of the BeamCal. To match the requirements on background suppression efficiency and Bhabha event identification high granularity and compactness is required in the BeamCal.

2.3 BeamCal as a Beam Monitor

The BeamCal, covering polar angles from about 4 mrad to 30 mrad, allows a bunch-to-bunch measurement of low-energy beamstrahlung pairs produced in the collisions. The deposited energy and its distribution depend on the actual beam parameters. The information can be used for a fast luminosity optimization by providing it to the beam delivery feedback system. The fraction of electrons and positrons from beamstrahlung hitting the BeamCal is about 5-10% of the total and amounts to about 10-20 TeV of energy per bunch crossing. Using the total energy deposits and several spatial asymmetries, information can be extracted not only on the overall luminosity achieved in each bunch collision, but also on the relative offsets between the bunches and on their sizes. Such information is essential to compute corrections then used by the beam delivery system, BDS, to optimize and maintain a high luminosity over a long time.

While the total amount of beamstrahlung pairs is not directly proportional to the luminosity, the relative information provided can be efficiently used for optimization following the "dithering" feedback approach pioneered at the SLC at SLAC [11]. With a more detailed analysis of the deposited energy profile, it has also been shown that both transverse and longitudinal beam sizes and transverse offsets can be reconstructed. A complete reconstruction of all these parameters simultaneously seems possible, however some of the parameters are highly correlated [12]. In this case the best results are achieved by combining the analysis with that of other diagnostic tools. For example, if the longitudinal beam sizes are known from measurements further upstream in the system, and if the measurements of the transverse offsets from beam-beam deflections are used, then the reconstruction of transverse beam sizes can be very precise. Another interesting method

is based on constructing suitable ratios of energies measured in different regions of the BeamCal. An example is provided in the method studied at KEK [13], which showed that excellent precision could be obtained on the vertical beam size by analyzing the azimuthal distribution of the energy profile.

Although it has not been fully demonstrated yet, it is expected that the amount of information which can be extracted from the BeamCal energy profiles will not depend significantly on the particular geometry chosen for the interaction region. Different detector magnetic field maps in the case of larger crossing angles [14] will however have impact on the distribution of the energy depositions on the BeamCal, hence the algorithms to extract beam parameters must be tuned for each configuration separately.

3 Systematics on Luminosity Measurement from Physics

3.1 Bhabha Scattering with Polarized Beams

To fully exploit the physics potential of the ILC, it is planned to equip it from the very beginning with a longitudinally polarized electron beam and, possibly a polarized positron beam. The beam polarization is expected to be 80% for electrons and about 60% for the positrons. The advantage of longitudinally polarized e^+e^- collisions is for example high precision analyzes of the SM, triple gauge couplings in $e^+e^- \to Z\gamma$, anomalous couplings in $e^+e^- \to W^+W^-$, structure analysis of the super-symmetric (SUSY) particles, extended SUSY models and other kind of new physics.

For longitudinally polarized colliding beams, the purely electromagnetic (EM) part of the Bhabha cross-section can be expressed in the center of mass system as

$$\frac{d\sigma_{EM}}{d\theta d\phi} = \frac{d\sigma^O_{EM}}{d\theta d\phi}\left(1 + P_- P_+ A^D_{EM}\right), \tag{1}$$

where $P_-(P_+)$ is the electron (positron) beam polarization and A^D_{EM} is the double spin asymmetry. The superscript 0 indicates the cross-section for non-polarized beams. When the electroweak (EW) contribution to the Bhabha scattering cross-section is non-negligible, in addition single spin asymmetry A^S_{EW} appears,

$$\frac{d\sigma_{EW}}{d\theta d\phi} = \frac{d\sigma^O_{EW}}{d\theta d\phi}\left(1 + (P_- - P_+)\, A^S_{EW} + P_- P_+ A^D_{EW}\right). \tag{2}$$

A^S_{EW} and A^D_{EW} depend on the initial energy, while A^D_{EM} does not.

The various single and double asymmetries are plotted in Figure 4 for the nominal beam energy of $E_{beam} = 250\,\mathrm{GeV}$. These asymmetries affect the total Bhabha scattering cross-section. In case of purely electromagnetic interactions, the integrated Bhabha scattering cross-section is

$$\sigma^{EM} = \sigma^{EM}_0\left(1 + P_{e^-} P_{e^+} f^{EM}_D\right), \tag{3}$$

where f^{EM}_D is the total electromagnetic cross-section asymmetry. Neglecting the electron mass we obtain

$$f^{EM}_D = 0.093\% \tag{4}$$

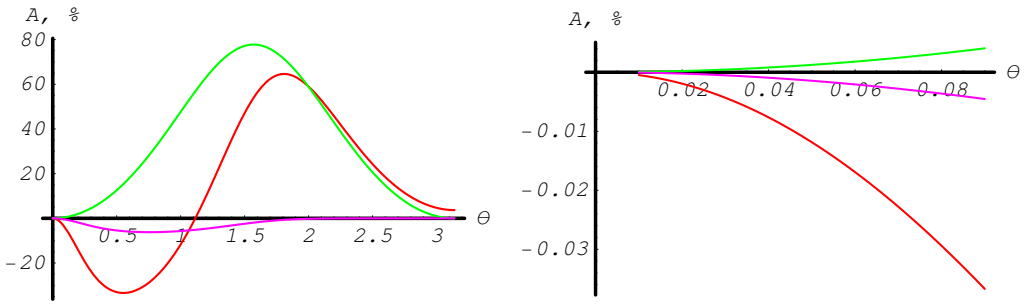

Figure 4: The spin asymmetries as a function of the polar angle θ. The left plot shows the full polar angle range, the right plot covers the range of the forward calorimeters. The green line is the result for A_{EM}^{D}, the red line for A_{EW}^{D} and the violet line for A_{EW}^{S}.

independent of the energy of the incoming beams. In the electroweak case, the total cross-section is given by

$$\sigma^{EW} = \sigma_0^{EW}\,(1 + (P_{e^-} - P_{e^+})f_S + P_{e^-}P_{e^+}f_D)\,. \tag{5}$$

The energy dependence of the asymmetries, f_S and f_D, integrated over the angular range of LumiCal, is shown in Figure 5. As can be seen, for beam energies of hundreds of GeV,

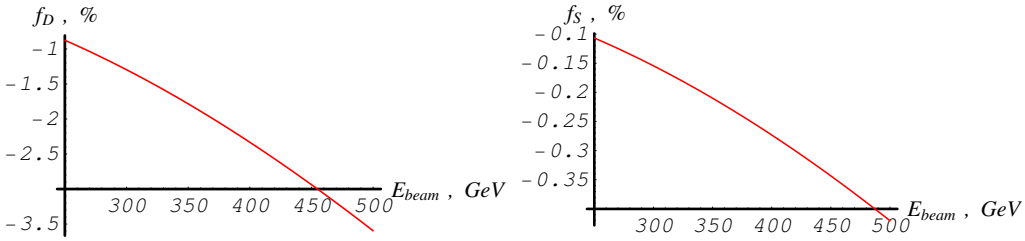

Figure 5: Double (f_D) ans single (f_S) spin asymmetries vs initial energy.

the polarizations of the beams change the Bhabha cross-section, integrated over the polar range of the LumiCal, by several per cent. Hence the polarization of the beams has to be taken into account in the measurement of the luminosity. In addition, it seems useful also to control polarization dependent higher order corrections.

3.2 Theoretical Precision of the Bhabha Monte Carlo Generators

For the final LEP results the theoretical cross-section uncertainty was the largest systematic uncertainty of the luminosity measurement [15]. Theorists are working in several laboratories to improve the accuracy of higher order corrections the the Bhabha cross-section [16]. In a recent report [17] the current theoretical uncertainty was estimated to be $5.3{\times}10^{-4}$ on the Z resonance, with the prospect to reduce this uncertainty to $2{\times}10^{-4}$, matching the

need of GigaZ. At higher energies the contributions of higher order corrections increase by several 10%, however, with sufficient effort, an uncertainty similar to the one on the Z-resonance should be feasible.

3.3 Impact of the Beam-Beam Effect on Bhabha Scattering

In Bhabha scattering, the beam-beam space charge effect modifies the energy and angular spectrum of the incoming and outgoing leptons. The spectra of the colliding beams can be calculated with the GUINEA-PIG program [18], one of the two tools dedicated to the simulation of beam-beam interactions.

Bhabha events are produced with BHLUMI 4.04 [19], in an angular range of $25 < \theta < 90$ mrad at 500 GeV center of mass energy, using the same parameters as in Ref [20]. We use the generated four-momenta list as input file for GUINEA-PIG. The particles transported through the volume of the bunch undergo the electromagnetic deflection. Primary particles lose energy due to beamstrahlung and kinematics has to be corrected to take into account that this leads to non-head-on collisions in the laboratory frame. In the analysis we consider Bhabha events where both final state particles are scattered into the FCAL angular acceptance of $26 < \theta < 82$ mrad. In addition, each detected particle is required to have an energy larger than 0.8 E_{beam}.

The Bhabha scattering cross-section is given to first order by

$$\frac{d\sigma_{Bh}}{d\theta} = \frac{2\pi\alpha^2}{s}\frac{\sin\theta}{\sin^4\theta/2} \equiv \frac{32\pi\alpha^2}{s}\frac{1}{\theta^3} ,$$

where α is the fine-structure constant, modified by its energy dependence, s is the center of mass energy squared and θ the scattering angle. Beam-beam interactions, which lead to beamstrahlung emission, modify the Bhabha scattering cross-section by lowering s and in addition, causes a small decolinearisation of individual electrons. The latter effect is estimated to be of the order of 10^{-1} mrad.

The bunch charge also affects the final state leptons. In particular, leptons produced under small polar angles, as typical of Bhabha scattering, follow a trajectory inside or near the incoming bunch and are focused by the bunch's electromagnetic field. The difference between the polar angle at the production point, θ_0, and after deflection by the bunch charge, θ_1, is shown in Figure 6 as a function of θ_0. The angular deflections amount to about 10^{-2} mrad and the smaller the θ_0, the larger the deflection. The leptons produced at polar angles slightly larger than the inner acceptance region of the calorimeter are deflected away from the acceptance region, while leptons with polar angles larger than the acceptance region are deflected into it. The number of leptons in the first sample is larger than the one in the second due to the θ dependence of the Bhabha cross-section. The net effect is the reduction of the number of Bhabha scattering events in the acceptance region. In the LumiCal acceptance region, typically 26 to 82 mrad, the effect amounts to $(0.48 \pm 0.03)\%$, using the nominal beam parameter set. If one reduces the angular acceptance to a range $30 < \theta < 75$ mrad the suppression effect is about $(0.36 \pm 0.03)\%$.

The Bhabha polar angle suppression effect depends on the beam shape. It is therefore important to find a correction method which would rely on a set of beam parameters and

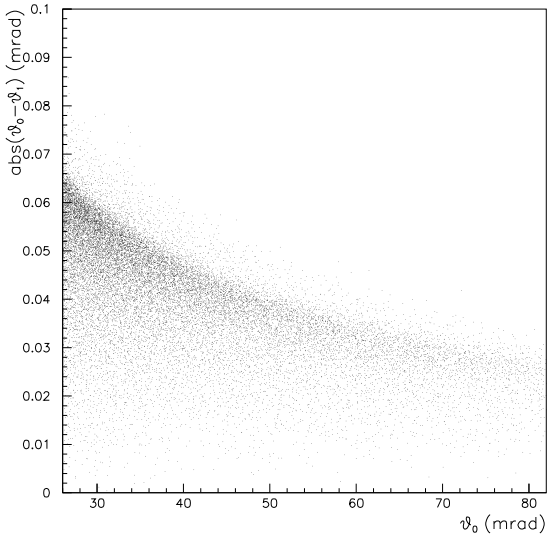

Figure 6: The shift in the polar angle due to bunch charge deflection, $\theta_0 - \theta_1$, as a function of the polar angle of the scattered Bhabha electron at the production point, θ_0. Both angles are in mrad.

to estimate the precision with which this correction can be evaluated.

3.4 Background to Bhabha Scattering

The signature of a Bhabha scattering event in the luminosity detector is an e^+e^- pair, where the leptons are back to back and carry almost all of the initial energy. Two photon events may fake Bhabha scattering when the additional fermion pairs are of low energy. We study as a source of physics background for luminosity measurement at the ILC the four-lepton processes, $e^-e^+ \to e^-e^+l^-l^+$ ($l = e, \mu, \tau$). The cross-section of these processes is dominated by multi-peripheral two-photon exchange, as shown in Figure 7. In these events, typically the electrons are scattered under small polar angles, mainly in the BeamCal angular region, and carry most of the energy, while the low energy lepton pairs are distributed over a wide angular range and end up in the LumiCal acceptance region as shown in Figure 8.

Preliminary studies of physics background [21, 22] have been performed at the generator level, using Vermaseren's generator [23] of two-photon processes, $e^-e^+ \to e^-e^+e^-e^+$, and the WHIZARD multi-particle event generator [24]. Based on samples of 10^3 events generated with Vermaseren's program and 10^5 four-lepton events generated with WHIZARD, both studies found an occupancy in the LumiCal acceptance region of 10^{-3} leptons per bunch crossing (BX).

A sample of 10^5 Bhabha scattering events was generated using BHLUMI simulation package, with the total cross-section of (4.58 ± 0.02) nb, assuming that electrons and positrons are produced within the polar angle range of $25 < |\theta| < 92$ mrad. For the

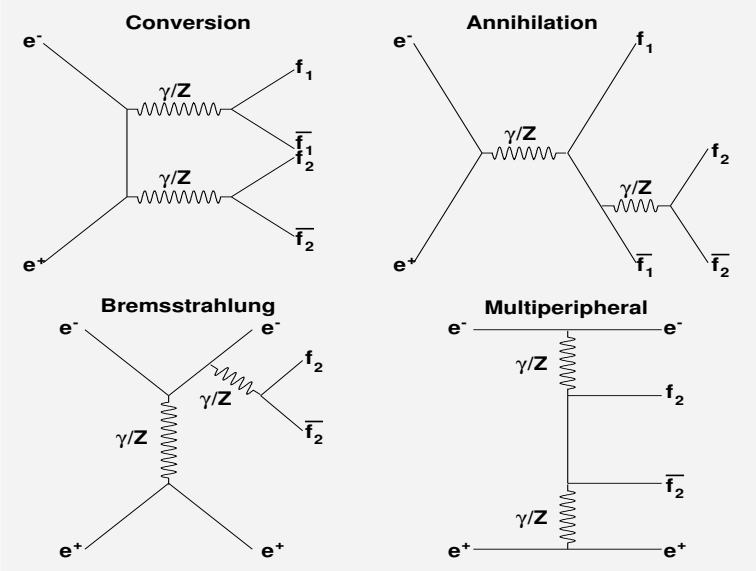

Figure 7: Feynman diagrams contributing to neutral current four-lepton production. The dominant fraction is described by the multi-peripheral diagram (bottom right)

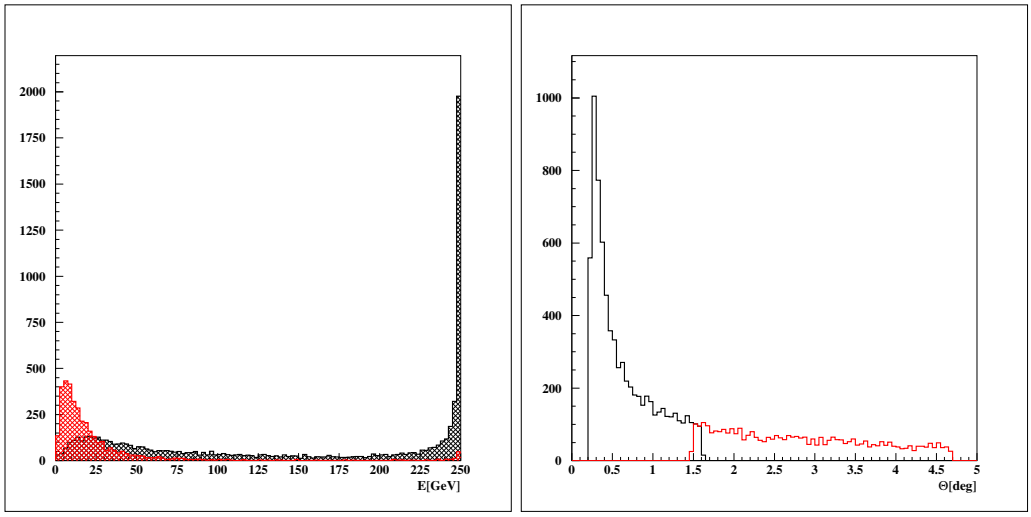

Figure 8: Energy and polar angle distributions of electrons from four fermion processes hitting the LumiCal (red) and the BeamCal (black).

design luminosity this cross-section corresponds to $9 \cdot 10^{-3}$ leptons/BX in the LumiCal acceptance region.

The response of LumiCal has been simulated using the BARBIE V4.1 [25] detector simulation package.

To simulate physics background a sample of 10^5 four-lepton events, $e^+e^- \to e^+e^-l^+l^-$ with $(l = e, \mu)$, has been generated with WHIZARD, with a total cross-section of (1.56 ± 0.03) nb for all neutral current tree-level processes. The simulation was performed in the polar angle range of 0.05^o to 179.95^o, with the invariant mass of the outgoing lepton pair greater than 1 GeV and the momentum transferred in photon exchange greater then 1 GeV. Though the cross-sections of the signal and background process are comparable, most of the background events can be rejected by typical selection criteria for Bhabha events. Bhabha events are characterized by a back-to-back topology and electron energies close or equal to the beam energy. We studied the effect of Bhabha event selection on the signal and background using the following set of cuts [26]:

- acolinearity cut $|\Delta\theta| < 1$ mrad,
- acoplanarity cut $|\Delta\phi| < 5^o$,
- energy balance cut $|E_R - E_L| < 0.1E_{min}$, where $E_{min} = \min(E_R, E_L)$ and E_R and E_L are the total energy deposited in the right (R) arm (front) and left (L) arm (back) of the LumiCal.

The distribution of hits projected on the front face of the LumiCal is presented in Figure 9, before and after applying the cuts. A signal to background ratio of 10^5 can be achieved with a loss of 20% of the signal. With a looser set of cuts,

- acolinearity cut $|\Delta\theta| < 8$ mrad,
- acoplanarity cut$|\Delta\phi| < 5^o$,
- relative energy cut $(E_L + E_R)/2E_{beam} > 0.75$,

one may achieve a rejection rate of 10^4 while preserving 98% of the signal. Hadronic two photon processes have not yet been studied, but we do not expect a dramatic change in the signal-to-background rate.

These preliminary results have shown that the background from two photon processes can be dropped to such a low level that the precision of the luminosity measurement will be maintained. Nevertheless, the study is ongoing, including all two-photon final states, a full detector simulation and more realistic beam conditions. One should note that the background from two photon processes contributes significantly to the occupancy of the LumiCal sensors. The latter may have an impact on the readout concept and requires further studies.

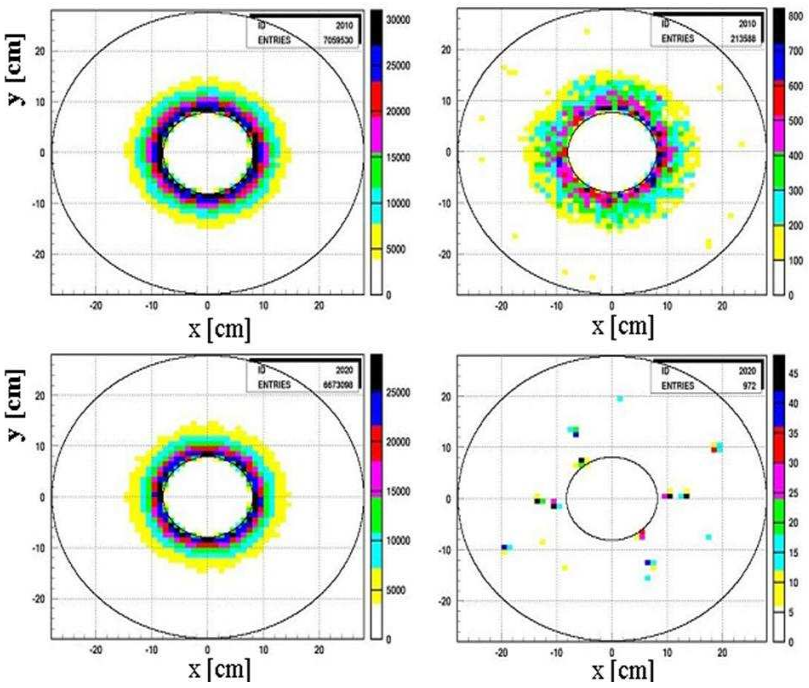

Figure 9: The distribution of hits at the front face of the luminosity calorimeter for Bhabha (left) and two photon events(right), before (up) and after (down) applying Bhabha event selection cuts.

4 LumiCal Progress Report

The present report includes all the studies performed after establishing a basic design for the LumiCal and the selection and reconstruction of Bhabha scattering events as described in the previous PRC report [27]. The LumiCal consists of two identical calorimeters positioned along the beam line, symmetrically with respect to the interaction point (IP), 3.05 m away from the IP. Each calorimeter covers polar angles θ from 26 to 92 mrad with respect to the beam line. Longitudinally, it consists of 30 layers composed each of 0.34 cm of tungsten and 0.31 cm of silicon and electronics. The active silicon sensor thickness is 500 μm. Each layer corresponds to a depth of about one radiation length. In the pad design, the calorimeter with an inner radius of 8 cm and an outer radius of 28 cm, is subdivided radially into 15 cylinders and azimuthally into 24 sectors. In the strip design, a readout plane subdivided into 64 concentric strips alternates with a plane consisting of 120 radial strips.

The events are selected based on the containment of the shower. After energy and position reconstruction, the latter based on optimized logarithmic weighting, tight selection cuts are applied as described in section 3.4. The energy resolution was found to be $\sigma_E = 0.25\sqrt{E}(GeV)$. For $E_{\rm beam} = 250\,{\rm GeV}$, the pad readout leads to a bias in the angle reconstruction, $\Delta\theta = 0.07$mrad and an angular resolution $\sigma_\theta = .13\,{\rm mrad}$. For the strip readout, $\Delta\theta = 2 \cdot 10^{-4}$ and $\sigma_\theta = 3.1 \cdot 10^{-2}\,{\rm mrad}$.

Since then, major progress was achieved in understanding the placement and performance constraints due to required luminosity precision, and in improving the pad design to match the performance of the strip readout. Digitization of the signal from LumiCal was introduced and the implication on the design of the readout electronics was investigated. Progress was made in designing the laser positioning system. No attempts were made to study the precision of energy calibration and energy resolution. Little progress has been made in the mechanical design.

4.1 LumiCal Placement Accuracy

The integrated Bhabha cross section is a strong function of the lower angular limit of the integration, $\theta_{\rm min}$,

$$\sigma_{\rm B} \sim \theta_{\rm min}^{-2}\,. \tag{6}$$

Any misalignment of the components of LumiCal or biases in the reconstruction of the scattering angle will influence the error on luminosity measurement.

To study constraints on the allowed misalignment of LumiCal [20], events were generated with BHLUMI. In a first step the position of the e^+ and the e^- on the front face of the LumiCal is calculated. The scattering angle is then deduced from these positions. The energy of the particles is taken from the generated four momenta and selection cuts are applied. The scattering angle constraint is applied to only one of the leptons, to e^+ for even events and to the e^- for odd events. Note that for any lepton to pass the energy cut, its scattering angle θ has to be in the range of LumiCal acceptance, that is $26.2\,{\rm mrad} < \theta < 82\,{\rm mrad}$.

In subsequent steps, the position and/or energy are subjected to systematic mis-reconstructions and the selection is reapplied. The change in the number of accepted events with respect

$\Delta L/L$	$0.2 * 10^{-4}$	$1.0 * 10^{-4}$
inner radius	0.8 μm	4.2 μm
radial offset	290 μm	640 μm
distance of calorimeters	76 μm	300 μm
longitudinal offset	8 mm	18 mm
tilt of calorimeters	6 mrad	14 mrad
beam tilt	0.28 mrad	0.63 mrad
beam size	negligible	negligible

Table 1: Parameter requirements to achieve the required precision on luminosity measurement [20].

to the number of originally selected events is a measure of the systematic effect induced by the particular mis-reconstruction. The size of the effects are varied in order to determine the required level of precision to achieve a goal of 10^{-4} uncertainty on the luminosity measurement. The same event sample is used for all steps so that statistical fluctuations largely cancel.

A selection of requirements thus obtained are presented in Table 1

4.2 Constraints on Angular Bias and Resolution

To achieve sensitivity to systematic effects comparable to the required relative precision on luminosity of 10^{-4}, large statistics MC samples are necessary. This cannot be achieved in a conventional manner, by processing events through a full GEANT [28] simulation. Instead, a fast MC was developed, with smearing effects implemented through parameterization of the performance established on smaller samples. The fast MC was coupled to the BHWIDE [29] event generator. This MC allows detailed studies of various systematic effects, either related to geometry or possible mismatch between MC simulation and detector performance.

The relative error on luminosity is proportional to the relative error of the Bhabha cross section

$$\frac{\Delta L}{L} = \frac{\Delta \sigma}{\sigma} \approx 2\frac{\Delta \theta}{\theta_{min}} . \tag{7}$$

The luminosity measurement is based on counting Bhabha scattering events in a well defined acceptance region. The error on the measurement is caused by miscounting events. The relative error on luminosity can then be written as

$$\frac{\Delta L}{L} = \frac{\Delta N}{N} = \frac{N_{rec} - N_{gen}}{N_{gen}}\Big|_{\theta_{min}}^{\theta_{max}} , \tag{8}$$

where N_{gen} is the number of generated events in a given angular range, and N_{rec} is the number of events reconstructed in the same angular range.

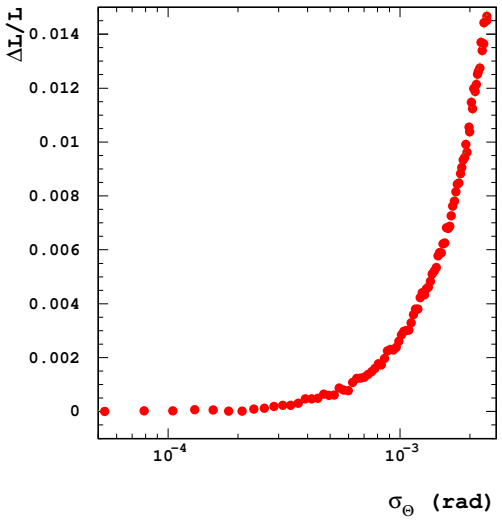

Figure 10: The relative error on luminosity, $\Delta L/L$, as a function of θ resolution, σ_θ, calculated using five million Bhabha scattering events for each point.

Two parameters describe the quality of the position reconstruction. One is the bias, $\Delta\theta$, and the other is the detector resolution (σ_θ). The limitation of $\Delta\theta$ can be easily obtained from the analytical formula and leads to a constraint of $\Delta\theta < 1.6 \cdot 10^{-3}$ mrad.

For the constraints on σ_θ, we used the fast MC. We smeared the generated events assuming a range of detector resolutions with zero bias. The influence of the detector θ resolution on the luminosity error is shown in Figure 10. $\Delta L/L$ is found to be a parabolic function of σ_θ.

From this parabolic dependence, one may derive the precision with which σ_θ has to be known to preserve the 10^{-4} precision on luminosity. For example for $\sigma_\theta = 1.6 \cdot 10^{-4}$ mrad, an error of $\pm 20\%$ would lead to an error on $\Delta L/L \simeq 0.4 \cdot 10^{-4}$. In conclusion, the most important issue is to be able to control the angular bias to below $1.6 \cdot 10^{-3}$ mrad.

4.3 Systematics Effects at Small and Large Beam Crossing Angles

The requirements on placement accuracy were reanalyzed for non-zero crossing angles. As the most critical parameter the control of the inner acceptance radius was identified and an accuracy of a few μm is required.

With a beam crossing angle, the detector axis usually has an angle of half the crossing angle with respect to the incoming and outgoing beams. We repeated the study on position accuracy requirements for two cases, the LumiCal centered around the detector axis and centered around the outgoing beam axis. When the LumiCal is centered around the detector axis the ϕ symmetry of the Bhabha cross section is lost. The Bhabha cross section in the laboratory frame depends then on the polar angle θ and on the azimuthal angle ϕ (see Figure 11), hence the systematic uncertainties become ϕ dependent.

Bhabha scattering is simulated for crossing angles of 2 mrad, 14mrad and 20mrad

using the BHWIDE and BHLUMI generators. Selection cuts, as described in section 2.6, are applied on the generated events and the number of Bhabha events is counted in the LumiCal acceptance region. Then the position or the geometry of the calorimeters were

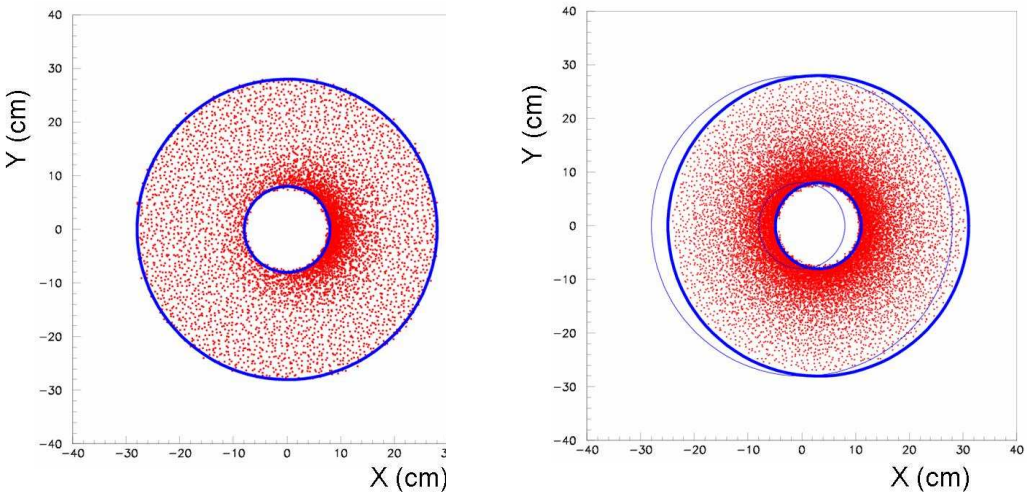

Figure 11: Distribution of Bhabha scattering events for the 20 mrad crossing angle ILC. Two cases are shown: the detector is positioned on the detector axis (left) and along the outgoing beam (right).

shifted in steps and the event selection was reapplied. The change in the number of accepted events with respect to the ideal geometry gives the systematic shift of the luminosity. The slope of the luminosity shift as a function of the shift of the parameter is a measure of the systematic sensitivity.

No significant difference in the systematic sensitivity between the two possible alignments of LumiCal were observed for shifts in the inner acceptance radius and in Z positions of the calorimeters. However, a dramatic change of the systematic sensitivity is found in case of larger crossing angles for radial beam axis sifts and for tilts of the calorimeter axes. Examples are shown in Figure 12. For a tilt of 0.1 rad, the relative change in luminosity, $\Delta L/L$, is strongly dependent on the angle ϕ and, if not corrected for, in the case of a 20 mrad beam crossing angle would change the measured luminosity for $\phi \approx \pi/2$ by almost 1 %. An even larger systematic sensitivity is observed for radial displacements of the beam axis as a function of the azimuthal angle ϕ. Note that, for small changes in the tilt or the radial beam position, for certain values of ϕ, the change in L is by more than an order of magnitude larger than the the anticipated precision of the luminosity measurement. Hence, in order to control the systematic uncertainty of the luminosity measurement, the LumiCal must be centered around the outgoing beam axis.

4.4 Optimization of the Pad Design

The new constraints derived on the allowed bias in the polar angle reconstruction were found to be two order of magnitude smaller than the bias obtained in the baseline LumiCal design

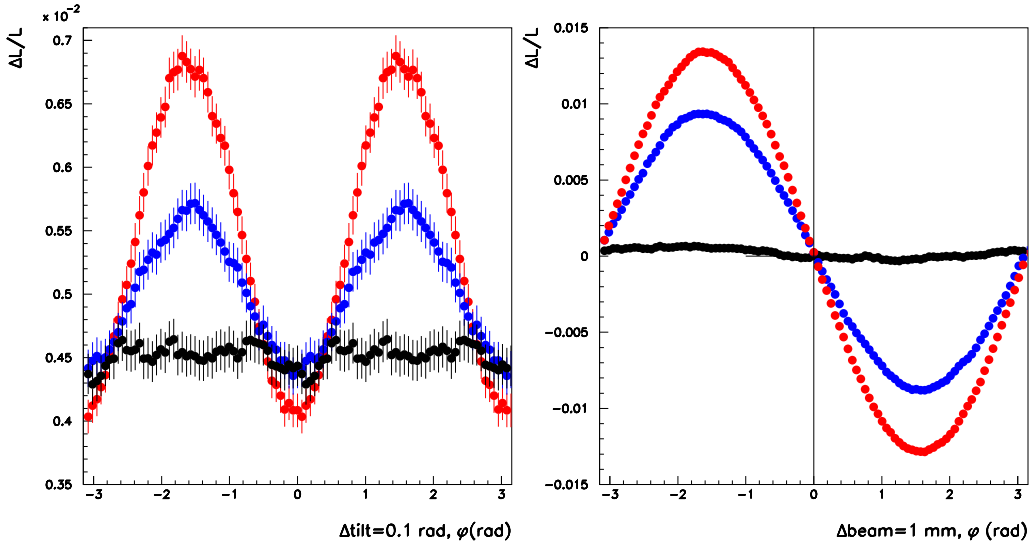

Figure 12: The relative shift in the luminosity as a function of the angle of tilts (left) and the angle of beam shifts (right) plotted for three cases: the LumiCal aligned on the outgoing beam (black), 14mrad ILC and the LumiCal aligned on the detector axis (blue), and 20mrad ILC while the LumiCal aligned on the detector axis (red).

with pad readout, described in section 1. The dependence of $\Delta\theta$ on radial granularity is shown in Figure 13. By increasing the number of cylinders from 15 to 60, one achieves $\Delta\theta = 1.4 \cdot 10^{-3}$ mrad as required. Such a granularity, if maintained throughout the whole depth of the calorimeter, would lead to an excessive number of readout channels. In order to reduce the number of channels an alternative design was considered, in which only the layers in the vicinity of the maximum shower position were to be finely granulated.

The proposal is to radially subdivide the layers as follows:

- 10 cylinders in the first four layers,
- 60 cylinders in the following 15 layers,
- 10 cylinders in the remaining 11 layers.

The expected performance of this shower peak design is summarized in Table 2, and compared to the performance of the strip design. Both designs fulfill the required precision in position reconstruction. The strip design is much more economical in terms of readout electronic channels, however the final decision will have to await more sophisticated studies of physics background and sensor properties.

4.5 Digitization of the Signal

In the strip design, the energy lost in the silicon strips was translated into charge deposits. The distribution of the charge deposit per cell is shown in Figure 14. The magnitude varies between 5 fC to 15 pC (0.5 to 2000 MIPS). The digitization of this large dynamical range requires 8 to 14-bit ADCs, depending on the required energy resolution. The performance

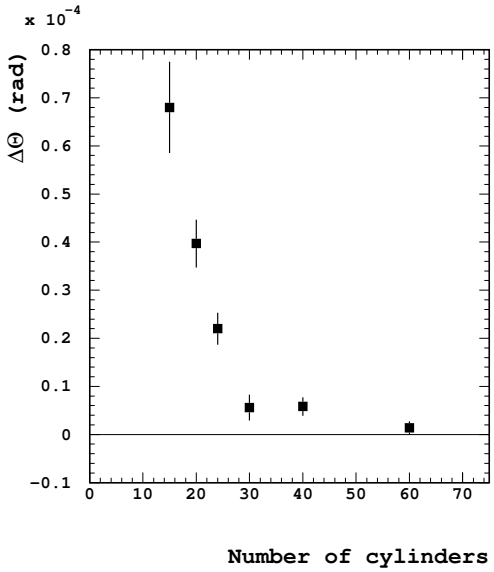

Figure 13: The polar angle bias, $\Delta\theta$, as a function of the radial granularity expressed in terms of the number of cylinders.

in position reconstruction was found to be the same for an 8-bit ADC as for the full energy loss information, as shown in table 3. Note, that since the same events were used for both methods, the errors are fully correlated.

It appears that the use of 8-bit ADCs would not deteriorate the performance of LumiCal . However, this conversion imposes a discriminating threshold of about 44 fC, which would mean that the detector is not sensitive to signals below 5 MIPS. This would preclude the use of muons for in situ alignment and calibration.

4.6 Digital Calorimeter

Confronted with the possibility to have to use expensive ADC solutions, we decided to investigate the performance of a possible digital LumiCal calorimeter. In the first attempt, each silicon plate was subdivided into 200 concentric rings and 720 radial strips, resulting in 14400 channels per plane. A hit was defined as an energy deposit of more than 1 MeV. Preliminary results show a good linearity in energy response, the energy resolution is comparable to that of the 'analog' calorimeter, σ_θ is factor 10 worse, and $\Delta\theta$ is by factor three worse. All in all, it seems a promising alternative, which we will pursue.

4.7 Background from Pairs for Non-zero Crossing Angle

One of the most important future benchmarks for the ILC is the crossing angle decision. A big crossing angle in the interaction region would complicate the luminosity measurement. The beam particles and backscattered particles will have a bigger transverse momentum in the region of the magnetic field and the total background will increase. One of the

Parameter	**Pad design**	**Strip design**
Number of electronic channels	25,200	8,000
Energy resolution	25%	
θ resolution (rad)	3.5×10^{-5}	2.1×10^{-5}
ϕ resolution (rad)	10^{-2}	10^{-3}
$\Delta\theta$ (rad)	1.4×10^{-6}	2.1×10^{-7}
$\Delta L/L$	$< 10^{-4}$	$< 10^{-4}$

Table 2: Summary of the expected performance of the alternative LumiCal designs.

Parameter	**analog**	**8-bit ADC**
θ resolution (mrad)	$(3.11 \pm 0.01) \times 10^{-2}$	$(3.07 \pm 0.01) \times 10^{-2}$
ϕ resolution (mrad)	1.4 ± 0.1	1.4 ± 0.1
$\Delta\theta/\theta$	$(2.1 \pm 0.03) \times 10^{-5}$	$(2.3 \pm 0.03) \times 10^{-5}$

Table 3: Performance in position reconstruction using analog signal and 8-bit ADC signal.

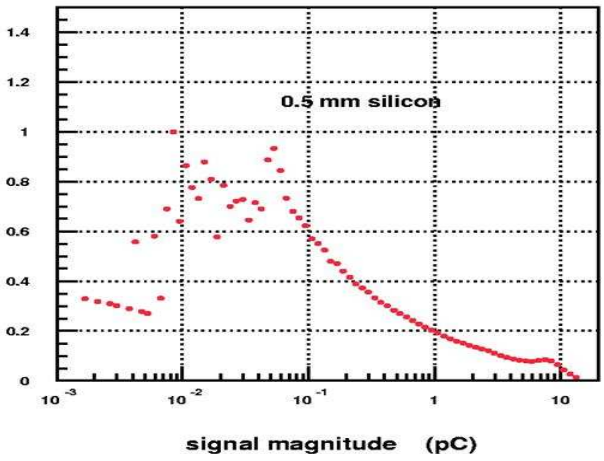

Figure 14: The signal magnitude distribution for 0.5 mm silicon sensors of the strip LumiCal.

challenges of this study will be to deal with the inhomogeneity and asymmetry in the ϕ angle of this background.

The recommended design for the head-on collision has a big acceptance region which offers the possibility to increase the inner radius and to get away from background close to the beam. Figure 15 shows the energy deposition per bunch, originating from beamstrahlung pairs, as a function of the LumiCal inner radius. This figure shows also the 'cost' in terms of statistics if the inner radius is increased. Above an inner radius of 13 cm there is no background and there is enough statistics to keep the statistical error on yearly luminosity smaller than the systematic one.

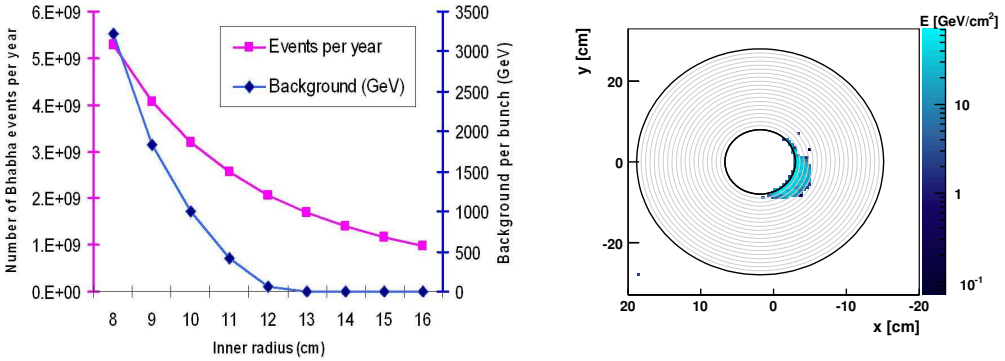

Figure 15: Left: background originating from beamstrahlung pairs (blue) and the number of expected Bhabha events per year (pink) as a function of the inner radius. Right: energy profile of beamstrahlung pairs hitting the face of Lumical.

4.8 Mechanical Structure

The two half barrels (arms) of the LumiCal can be clamped on the beam pipe. The position of each arm of the detector will be fixed using precise pins located at the top and bottom of a C shaped steel frame. The latter stabilizes the structure and carries the heavy tungsten disks on one set of bolts and the light silicon sensors will be glued to a ceramics support by a separate set of bolts. This way, the sensors frame is decoupled from the tungsten disk support, hence it does not suffer the gravitational sag due to the tungsten weight. The silicon sensors of 300 μm thickness are glued on a 1 mm thick ceramic support and a 0.7 mm space is left for bonding and for kapton foil with readout traces. A place for readout electronics, connectors and cooling is foreseen as shown in Figure 16.

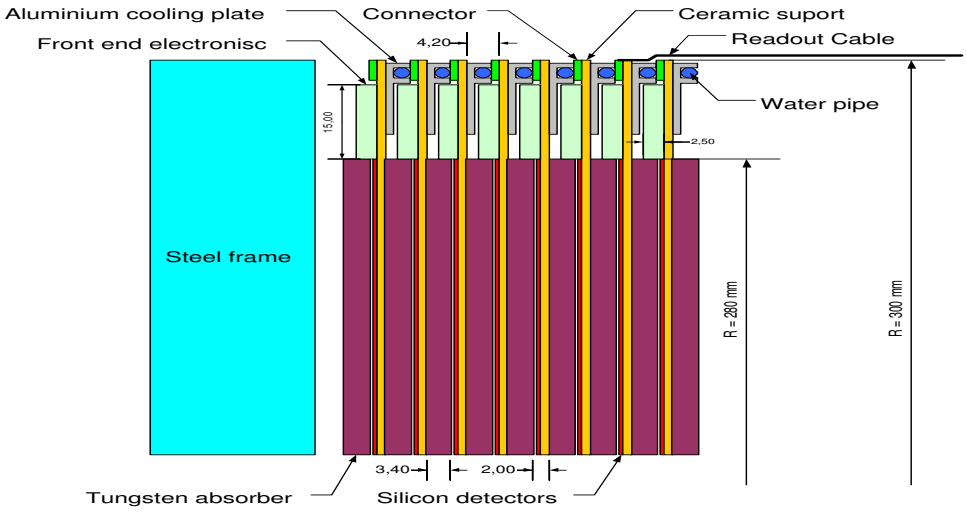

Figure 16: Proposal for the mechanical design of LumiCal.

A thin water pipe goes round the outer detector diameter, pressed into the aluminum radiator glued to the bottom side of the ceramic sensors support. The thickness of the radiator will be chosen such as to enable electronic contact on subsequent disks, also from the top. The silicon sensors have to be positioned with μm precision and an on-line precision optical survey is foreseen. The holes in the C shaped frame will carry the laser light through the semi-transparent position sensors placed on each ceramic support. The thermal stability of the mechanical structure has to fulfill the extreme precision requirements for the sensors positioning. A constant temperature of the detector can be obtained by stabilizing the cooling parameters.

4.9 Alignment and Position Monitoring

The luminosity measurement requires extremely precise alignment of the two LumiCal detectors, each with respect to each other, and a very precise positioning with respect to the beam line and the interaction point. Monte Carlo simulations have shown [20] that the inner radius of sensor layers has to be known with an accuracy better than $4\,\mu$m, the distance between calorimeters along the beam axis must be known to a accuracy of 60 μm over a 6 m distance and the transversal displacement (x, y) with respect to the beam is required to be known to 100 μm accuracy. Initially, the inner radius of the detector can be measured in the lab using optical methods.

The beam pipe is proposed as a suitable reference for the distance along the beam and the transversal displacement, and can be precisely surveyed before installation, under different conditions (i.e. temperature). The temperature and tension sensors should be installed on the beam pipe to control and correct the mechanical dimensions. The Beam Position Monitors are mounted at a well known position inside the vacuum pipe and that would allow to determine the actual position of LumiCal with respect to the beam position. The position monitoring of the detector should not interfere with the beam pipe, hence a non contact system is preferred.

We have chosen an optical laser system with a CCD matrix sensor to measure the transversal (x, y) and longitudinal (z) displacement of the LumiCal with respect to the beam pipe flange. The position sensors will be placed between the rear side of the detector and the beam pipe flange. The radiation dose in that area seems to be small because of shielding, but the radiation hardness of the sensor has to be studied. In case the radiation dose will not acceptable, we can use radiation hard CMOS matrix sensors. The use of a few additional position sensors per calorimeter would allow to determine also the angle between the detector axis and the beam direction, and would ensure better redundancy.

We have set up an experiment using the semiconductor laser module LDM635/1LT from Roithner Lasertechnik with a wavelength of 660 nm and BW camera, DX1-1394a from Kappa company, 640 x 480 with Sony ICX424AL sensor and a $7.4 \times 7.4\,\mu$m unit cell size. The laser was mounted in a special precision alignment holder on the optical bank. The camera was placed on the XYZ ThorLabs travel translation stage MT3 with micrometers (smallest div. 10 μm). We had to reduce the amount of laser light using three neutral density filters with the attenuation factor of two, each because the sensor saturated.

The camera was translated in one direction in 50 μm steps and a picture was taken. Two algorithms to calculate the center of the beam spot was developed and both gave similar results. The results are shown in Figure 17 and the difference between the real and the calculated position was found to be less than $\pm 2.5\,\mu$m. Part of this difference must be due to uncertainties of the micrometer screw. We have made a few series of measurements an the results were stable. To measure the longitudinal (z) displacement we intend to use a second laser beam, lighting with an angle of 45 degrees with respect to the sensor (see Figure 18).

We have used a half transparent mirror to split the laser beam and another mirror to direct it to the sensor with a proper angle. First measurements of the z displacement show that the calibration of the mirror angle is crucial for the final accuracy.

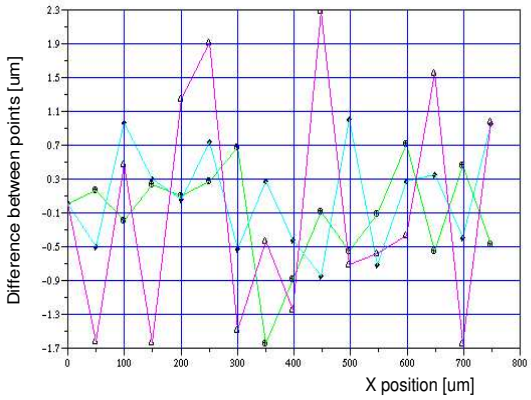

Figure 17: Position measurement results obtained using a camera and a laser light.

A new setup, shown in Figure 19, with a special prism has been developed and ordered. We have also designed a special holder for two lasers instead of splitting the laser beam. A work on displacement sensor miniaturization has started. We have chosen a CCD fine pixel sensor and the readout electronics has been designed. The PCB is under design. Not only a full detector has to be aligned precisely, but also the position of the sensors planes has to be known within a few μm. We foresee an optical system to control online the displacement of the sensor planes, as shown in Figure /reffigg.

The laser beam from a semiconductor laser module placed in the hole of the C shape steel frame goes through semitransparent CMOS position sensors (similar to the sensors used in CMS). Another possibility is to use a wire extended between the front and rear C shape steel frame passing through the holes in all detector planes. Simple capacitive sensors can measure the transversal displacement of the sensor planes with respect to the wire.

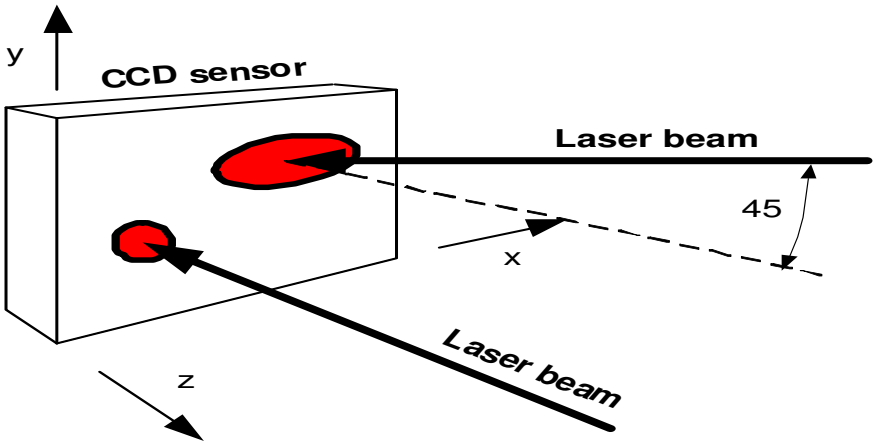

Figure 18: Setup to measure x,y and z displacements.

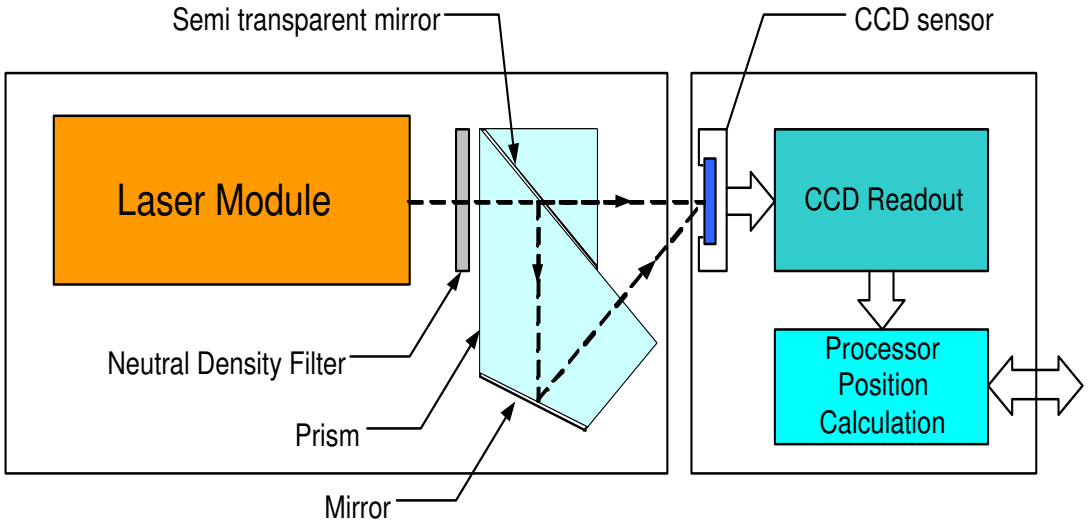

Figure 19: New setup for position monitoring.

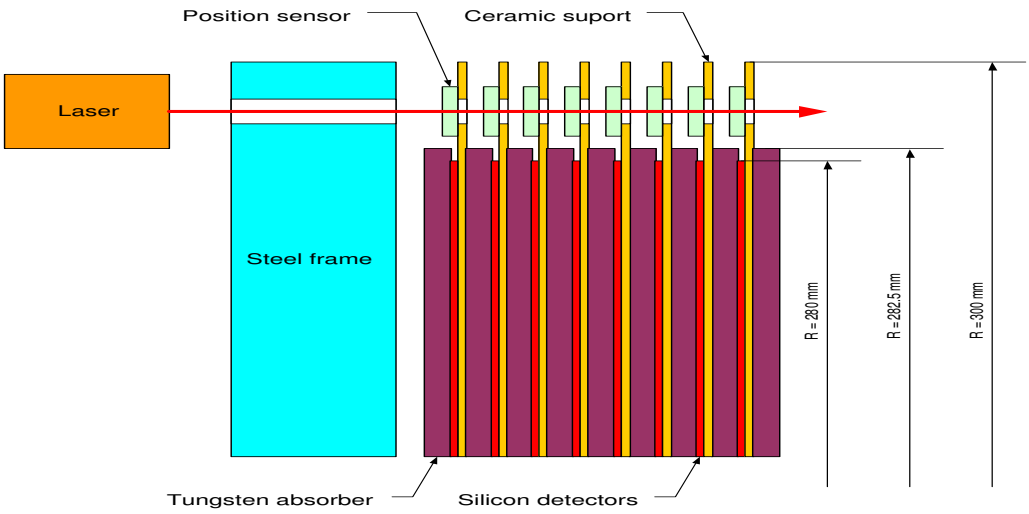

Figure 20: Monitoring system for the inner sensor planes position.

5 The BeamCal

5.1 ILC Parameters and Beam Crossing Angles

The ILC accelerator parameters are still under discussion in the world-wide community. As will be shown, the BeamCal design will depend on the beam crossing angles and its performance for high energy electron detection will depend both on the crossing angle and the accelerator parameter sets. We propose here BeamCal versions for a small (2 mrad) and a large (20 mrad) crossing angle and report about the performance studies done.

As it is pointed out in Ref. [10], the TESLA machine parameters were chosen to achieve a high peak luminosity accepting a large disruption parameter. As a more flexible approach it is proposed to define an operating parameter space, where a number of different machine operation schemes achieve the same peak luminosity. We consider here the impact of these schemes on the pair depositions in the BeamCal.

For a 2 mrad crossing angle the depositions of pairs on the BeamCal are very similar to the ones of the head-on scheme. The only change to be done for the BeamCal is a slightly larger inner radius.

The 20 mrad crossing angle concept is discussed for several versions of the magnetic field inside the detector. In the DID[2] field configuration the magnetic field is directed along incoming beam lines with a kink at the transverse plane containing the IP. The incoming beams will not suffer by synchrotron radiation and spin precession before they collide. However, the amount of beamstrahlung deposited in the BeamCal rises considerably, causing also higher background in the tracking detectors due to backscattered particles. Conversely, if the magnetic field is directed along outgoing beam lines with a kink at the IP-plane, called Anti-DID, the depositions on the BeamCal and background in the central detector are very similar to the head-on case. To reduce the interaction of the incoming beams with the magnetic field a crossing angle of 14 mrad is suggested.

5.2 Experimental Situation

The BeamCal will be hit by the electrons and positrons originating from beamstrahlung photon conversions, carrying several 10 TeV of energy per bunch crossing for nominal beam parameters. The distribution of this energy is shown in Figure 21. The energy density is largest at small calorimeter radii and strongly dependent on the azimuthal angle. The latter is the result of the flat beam and the helical trajectory of electrons and positrons in the magnetic field inside the ILC detector. With growing radius the energy density drops showing a sharp border of the affected area, though a smaller number of particle can be found at larger radii.

As it is explained in detail above, high energy electron identification is particularly important to veto backgrounds to new particle searches. Fine granularity is necessary to identify the localized depositions from high energy electrons and photons on top of the energy depositions from beamstrahlung remnants. Sharing the shower signal between neighboring segments will improve the position resolution. Since the beamstrahlung energy

[2]Detector integrated dipole

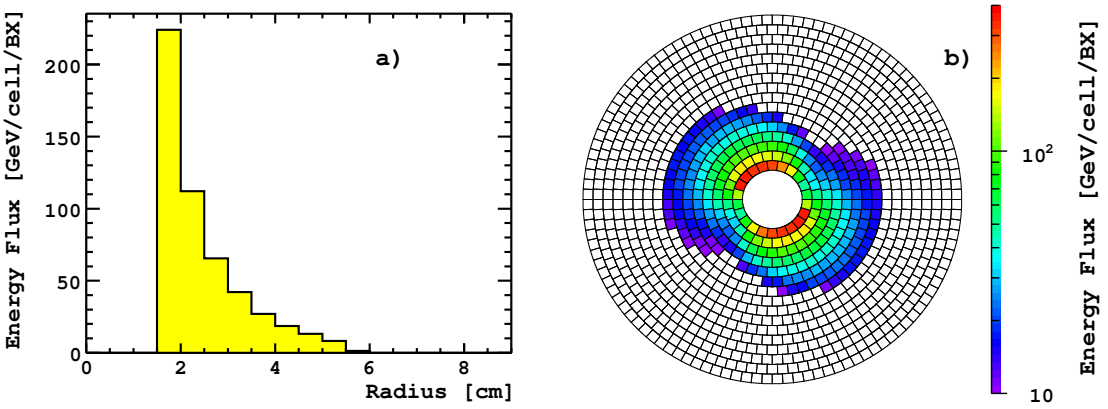

Figure 21: The energy density of beamstrahlung remnants per bunch crossing as a function of a) radius and b) position in the $r-\varphi$ plane. The centre-of-mass energy is 500 GeV. The maximal value of the density is 350 GeV per cell.

deposition varies considerably with R and φ, and fluctuates from bunch to bunch, a dynamic range of $\mathcal{O}(10^3)$ is required.

The reconstruction efficiency of single electrons was studied for the diamond-tungsten sandwich calorimeter and the crystal calorimeter [27]. The first is chosen as baseline due to its superior veto efficiency. The simulations reported here are based on this technology choice.

The simulated sampling calorimeter is longitudinally divided into 30 disks of tungsten, each 1 X_0 thick (3.5 mm) interleaved by active sensor layers of 0.5 mm thickness. The Molière radius is about 1 cm. The sensitive planes are divided into pads with a size of about half a Molière radius in both dimensions, as shown in Figure 21b.

Head-on and 2 mrad schemes foresee 1 beam-pipe. In case of a large crossing angle incoming and outgoing beams need separate beam pipes. The BeamCal is assumed to be centered on the outgoing beam. The instrumentation of the small region between the beam pipes is technically difficult and we assume that a sector containing the incoming beam-pipe will not be instrumented. Table 4 summarizes the BeamCal geometries we assumed for the various crossing angle schemes.

scheme	R_{in} [mm]	R_{out} [mm]	blind area
head-on	15	100	no
2 mrad	20	100	no
14 mrad	15/20	165	40°
20 mrad	15/20	165	30°

Table 4: Geometries of the BeamCal for various crossing angle schemes. For large crossing angle cases the two given inner radii specify the opening for the incoming/outgoing beam.

5.3 BeamCal Physics Potential and Design Study

The beamstrahlung pairs and single electrons are generated and tracked through the detector. The energy depositions from the pairs and the single electron in the sensor pads are superimposed. The depositions on all pads are then used in a shower reconstruction algorithm. Beamstrahlung is generated using the GUINEA-PIG generator. The detector is simulated using the GEANT4 [30] software package. The simulations are done for the different accelerator parameter sets and for different crossing angles. The centre-of-mass energy is 500 GeV.

The electron detection performance is used to estimate the suppression of two-photon background in the different accelerator schemes. The search for the stau SUSY particle, as described above, is taken as a benchmark process. Furthermore, effective luminosity reduction due to electron vetos induced by incomplete reconstructed or radiative Bhabha events is estimated. The electron detection performance is studiedas a function of the sensor pad size and the dose collected in the sensors of the BeamCal for the different accelerator parameter sets is estimated.

5.3.1 Physics Requirements and Detector Performance for the Electron Veto Performance

After applying all selection cuts except the electron veto 20 stau events are left, while the number of surviving 2-photon background events is about 2.7×10^5. Figure 22 shows the energy and spatial distribution of the electrons originating from the two photon events. Most of these electrons have nearly the beam energy and hit the BeamCal outside the area affected by pairs, though the distribution has tails down to the smallest angles and energies. It is important to notice that the distribution depends on the mass difference between the stau and the neutralino, e.g. if it is larger than 5 GeV the distribution is broader and shifted to larger angles.

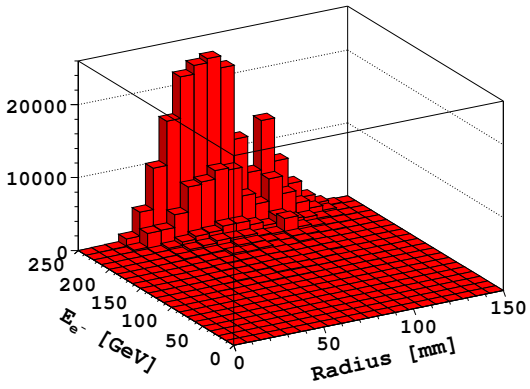

Figure 22: Electron energy and spatial distribution of the 2-photon background events passed all cuts except veto.

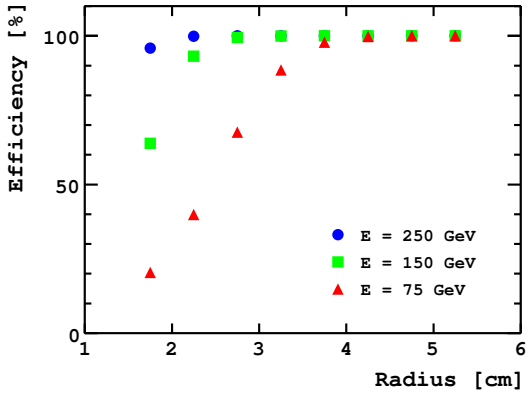

Figure 23: The efficiency to identify an electron of energy 75, 150, 250 GeV as a function of the radius in the BeamCal.

The average efficiency to veto electrons is shown in Figure 23 for several electron energies at head-on collision and nominal beam parameters. An electron of 250 GeV is vetoed even in regions with high background with almost 100% efficiency. The efficiency drops near the innermost radius, partly due to shower leakage. Electrons of 75 GeV are identified with high efficiency only at larger radii.

Performing the reconstruction, fake electrons can be found. This can be either a high energetic particle originating from beamstrahlung or background fluctuations which mimic the electron signal. In this study the reconstruction algorithm is tuned such that the rate of fake electrons is below of 10%.

5.3.2 Two-photon Background Suppression at Various Beam Parameter Configurations

In Table 5 the beam parameters for different accelerator designs are given for 500 GeV centre-of-mass energy[10].

	Nominal	LowQ	LargeY	LowP
Bunch charge [10^{10}]	2	1	2	2
Number of bunches	2820	5640	2820	1330
Gradient [MeV/m]	30			
$\gamma\epsilon_x/\gamma\epsilon_y$ [10^{-6} mrad]	10 / 0.04	10 /0.03	12 / 0.08	10 / 0.035
β_x / β_y [mm]	21 / 0.4	12 / 0.2	10 / 0.4	10 / 0.2
σ_x / σ_y [nm]	655 / 5.7	495 / 3.5	495 / 8.1	452 / 3.8
σ_z [μm]	300	150	500	200
Luminosity [10^{34} cm^{-2}s^{-1}]	2.03	2.01	2.00	2.05

Table 5: Beam parameters for the different accelerator designs at $\sqrt{s} = 500$ GeV.

For each beam parameter set in Table 5 veto efficiencies as shown in Figure 23 are estimated from simulations. These efficiencies where included into the stau search analysis. The number of unvetoed 2-photon events for each beam parameter set is listed in Table 6. Results are given for energy cuts of 50 and 75 GeV, showing that a relatively low energy cut of 50 GeV improves the signal-to-noise ratio considerably. For the chosen benchmark physics scenario the chances to see stau particles are very good for most of the accelerator designs. Only for the LowP scheme the remnant background dominates the selected event sample. By far the best situation is given for the LowQ scheme.

5.3.3 Two-photon Background Suppression for the Different Crossing Angle Options

The distribution of depositions from beamstrahlung pairs on the BeamCal is very similar for 2 mrad and 20 mrad beam crossing angles provided in the latter case the anti-DID field is used in the detector. For a 20 mrad beam crossing angle with a DID field the deposited energy, for each of the accelerator parameter sets, is much larger and the shape

Energy cut [GeV]	75	50
Nominal	45	5
LowQ	40	0.1
LargeY	50	9
LowP	364	321

Table 6: The number of background events after applying the veto for high energy electrons in the BeamCal. The number of expected stau events is for all cases 20.

of the distribution, shown in Figure 24b, is different. We can assume that the BeamCal performance for crossing angles of 2 mrad and 20 mrad with Anti-DID field are similar and also similar to the head-on case. Hence we study now the performance of the BeamCal only for the 20 mrad beam crossing angle case. The study of stau production as described

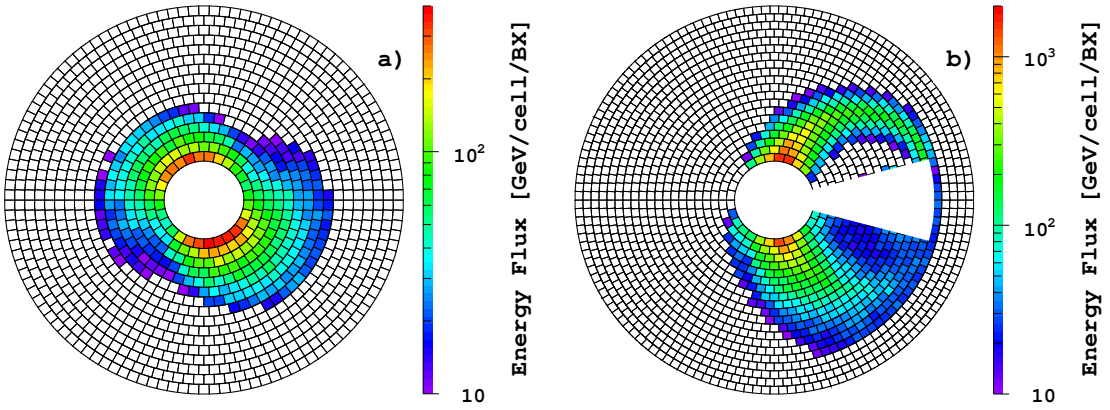

Figure 24: The energy density of beamstrahlung remnants per bunch crossing as a function of position in the $r - \varphi$ plane at the a) 2 mrad and b) 20 mrad with DID field crossing angles.

above is repeated. The number of unvetoed 2-photon events remaining in the analysis is 349 compared to 5 events in the case of head-on collisions. The number of stau events is again 20 in both cases. Hence, for this particular benchmark scenario we would have no chance to see stau production at 20 mrad crossing angle and a DID field.

5.3.4 Effective Luminosity Reduction Due to not Identified Bhabha Events

The Bhabha rate grows very rapidly for decreasing polar angles and becomes large in the BeamCal range. As it is shown above, the identification of high energy electrons becomes inefficient near the beam-pipe. Hence it may happen that only one electron is reconstructed for a Bhabha event. In addition, radiative Bhabha events may have one electron inside and the second outside the BeamCal acceptance region. These Bhabha events fake the signature of a two-photon events, and we would suppress them in the analysis to search e.g for staus, dropping effectively the luminosity available for a certain search experiment.

To estimate this effect, a simulation is done for the crossing angle schemes head-on, 2 mrad and 20 mrad with DID field. The Monte Carlo programs BHLUMI and TEEGG [31] are used for Bhabha event generation[3]

The generated Bhabha events are fully simulated on top of the beamstrahlung depositions and then is applied the reconstruction algorithm for single electron showers.

The number of identified Bhabha events and single electron Bhabha events per bunch crossing in the BeamCal acceptance range is shown as a a function of the calorimeter radius [4] in Figures 25a and 25b), respectively, for different beam crossing angles. The veto rate due to Bhabha scattering is about 5% for zero or 2 mrad crossing angle and roughly 15% for 20 mrad crossing angle.

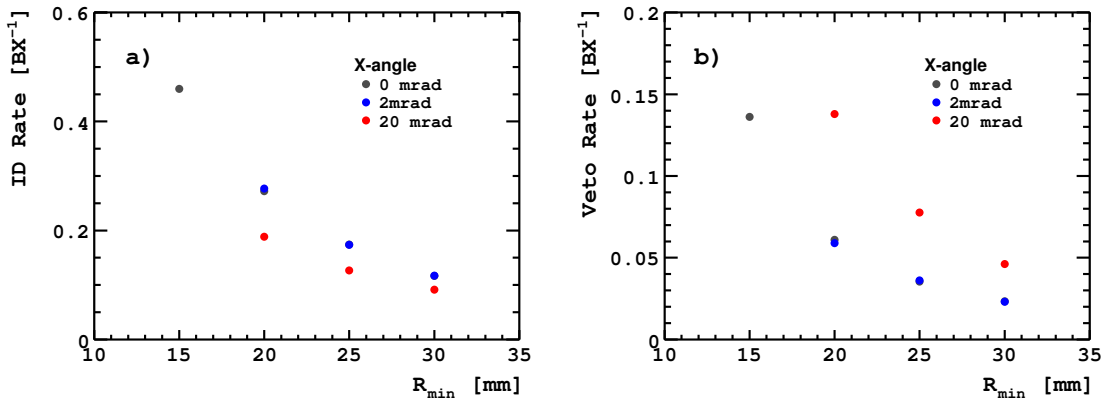

Figure 25: a) Bhabha identification rate and b) Bhabha induced veto rate in the BeamCal as function of the minimal acceptance radius for various crossing angle schemes.

5.3.5 Transversal Segmentation

The efficiency to identify high energy single electrons as shown in Figure 23, is the essential performance parameter of BeamCal. In particular in the inner part of the BeamCal the efficiency decreases due to beamstrahlung depositions. We studied this efficiency for sensor pad sizes between 4×4 and 10×10 mm^2. The result is shown in Figure 26 for the inner part of BeamCal. The inefficiency for the identification of 200 GeV electrons, plotted as a function of the pad size, has a shallow minimum around 5×5 mm^2, corresponding to about half a Molière radius.

[3] At very small polar angles BHLUMI is not prepared to simulate radiative Bhabha events properly. We therefore used BHLUMI above a certain polar angle threshold and the TEEGG generator below this threshold.

[4] These are cumulative distributions, the number of events per bunch-crossing for a certain radius contains all events hitting the calorimeter above this radius.

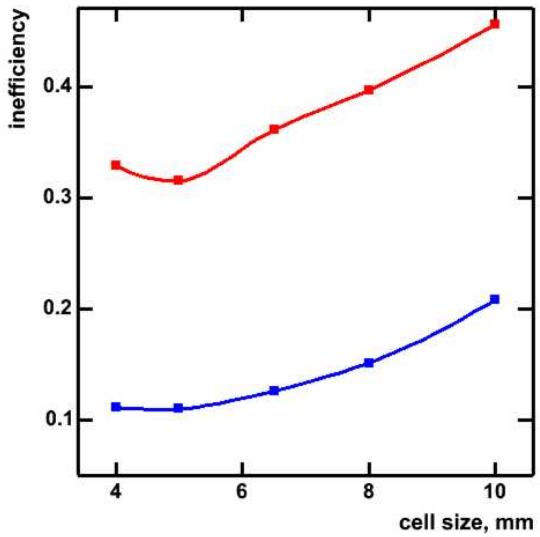

Figure 26: The inefficiency to detect electrons of 200 GeV as a function of the size of the sensor pads. The blue and read curves are obtained for regions of low and high background, respectively.

5.3.6 Expected Doses for Different Beam Parameter Sets

The energy deposited in the volume of each sensor pad is averaged over beamstrahlung pair depositions of 500 bunch crossings and then multiplied by the number of bunches per year. The simulation is done for all beam parameter sets. The distributions for the two extreme cases, LowQ and LowP are shown in Figure 27. The Nominal and LargeY parameter sets result in doses in between them. There is a large difference in the dose itself and in the size of the affected area for LowQ and LowP parameters. The maximum doses are 0.44 MGy/year and 4.3 MGy/year for LowQ and LowP parameter sets, respectively.

5.4 Beam Diagnostics

Analyzing the energy deposition from Beamstrahlung pairs has a large potential to optimize the machine operation for the largest luminosity of the collider. Albeit not directly proportional to the luminosity, the signal from the pairs can be a fast indicator of the collision quality. If a signal like the number of pairs hitting the BeamCal is included into the feedback system [32] the overall luminosity can be increased by 12% and more [33]. This fast or instantaneous luminosity signal has to be provided within a few bunch crossings.

A thorough analysis of the shape and energy spectrum grants access to parameters of the initially colliding beams, as it has been described in detail in [27, 12]. The Monte Carlo generator GUINEA-PIG is used to simulate the bunch-bunch interactions. A FORTRAN based software is then used to track the generated electron positron pairs through the magnetic field of the detector, which is assumed to be homogeneous and of ideal res-

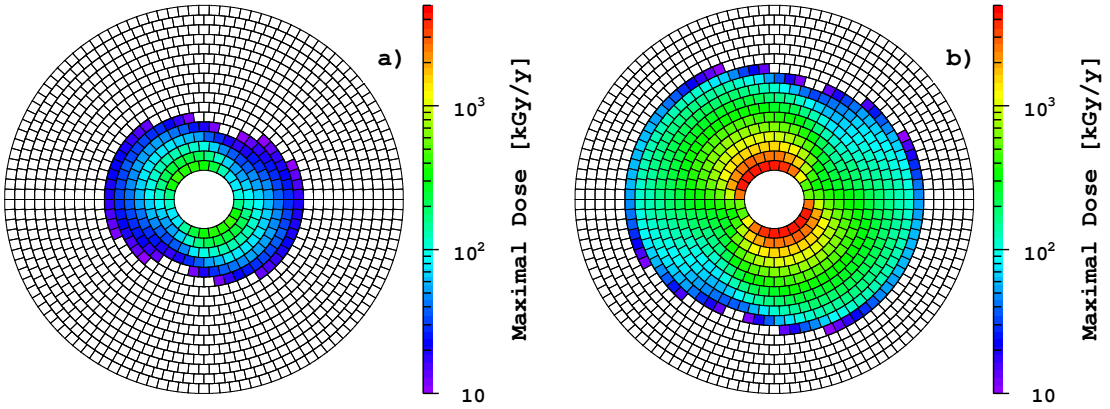

Figure 27: The expected dose in the most suffered longitudinal cell as function of position in the $r - \varphi$ plane at a) LowQ and b) LowP beam parameter configuration.

olution. The energy of the particle is added to the corresponding BeamCal segment at the impact position. By simulating the variation of individual beam parameters like beam sizes, emittances, offsets and bunch charge the correlation between beam parameters and observables can be found in the approximation of a first order Taylor expansion. Inverting the Taylor matrix by calculating the Moore-Penrose inverse then allows one to determine beam parameters from a set of measured observables. The investigations presented in the last PRC report are based on TESLA parameters and a crystal calorimeter geometry.

The analysis was repeated using the new beam parameters, crossing angles and the corresponding magnetic field. The pad size of the BeamCal sensors has been chosen for this purpose to be $0.8\,\mathrm{R}_M$ in both dimensions, leading to a reasonable veto efficiency but reducing the overall channel number considerably. The segmentations and a typical deposition for nominal ILC beam parameters are shown in Figure 24 for 2 mrad and 20 mrad with DID like magnetic field.

In table 7 the precision obtained for the beam parameters for 2 and 20 mrad, the latter with a DID magnetic field, are shown using the Moore-Penrose inversion method. The precision is slightly worse for the large crossing angle, nevertheless very promising. An optimization of the set of observables for this case has still to be done. The variation of two and more beam parameters at the same time is possible, as shown in the "dbl" column of the table, with a slighly worse precision.

The use of the reconstruction algorithm with a realistic detector response and showering is currently under study. A GEANT4 based simulation has been set up featuring variable crossing angles and detector segmentations, as well as the usage of a more realistic magnetic field map. The simulation of one bunch crossing takes about 250 min on a Dual Xeon 3.2 GHz computer with 2 Gbyte RAM. This still is feasible for farm processing of the first order Taylor matrix coefficients, which corresponds to about 400 bunch crossings. A fast shower parametrization is therefore not required. In a next step the data from the full simulation will be used for a beam parameter reconstruction and the investigation, if a subset of the BeamCal information, is sufficient to reach a good precision.

beam parameter	unit	nominal	2 mrad sngl	20 mrad DID sngl	20 mrad DID dbl
σ_x	nm	655	3.1	2.9	2.8
$\Delta\sigma_x$	nm	0	5.2	7.4	7.6
σ_y	nm	5.7	0.3	0.2	0.2
$\Delta\sigma_y$	nm	0	0.3	0.4	0.4
σ_z	μm	300	4.8	8.5	11.1
$\Delta\sigma_x$	μm	0	3.7	6.3	7.4
ε_y	μm mrad	40	1.7	2.9	5.2
$\Delta\varepsilon_y$	μm mrad	0	4.2	4.1	4.7
Δx	nm	0	17.7	9.3	10
Δy	nm	0	0.5	0.6	0.6
N	10^{10}	2.0	0.01	0.01	0.01
ΔN	10^{10}	0	0.01	0.02	0.03

Table 7: Precision of the beam parameter reconstruction for small and large crossing angle (with DID magnetic field). Given beam parameters are: beam sizes (x, y and z) , emittance in y, beam offset in x and y and bunch charge. Each beam parameter is given as average and difference of the two beams. For the large crossing angle the precision of a double parameter analysis is also given, where average and difference of a beam parameter are reconstructed simultaneously.

6 The PhotoCal

Photocal will measure the photons from beamstrahlung which are emitted at the IP with smallest polar angles of several 100 μrad and is therefore positioned at a distance of 100-200 m downstream from the IP. A heavy gas (C_3F_8) ionization chamber is foreseen as the detecting layer as it was described in [27]. By analyzing the tails of the beamstrahlung photon distribution (≥ 100 resp. 400 μrad) information about the collision can be obtained.

The studies are ongoing but there are no new results to report on.

7 CVD Diamond Studies for BeamCal

Large area polycrystalline diamond sensors are thought to be very radiation hard and are therefore a promising sensor material for the Beam Calorimeter. The studies are done in collaboration with the Fraunhofer Institute für Angewandte Festkörperphysik (Fraunhofer IAF), and aimed to the production of high quality polycrystalline Chemical Vapor Deposition (pCVD) sensors appropriate for the Beam Calorimeter application.

The studies include measurements of the electrical properties of the pCVD diamond sensors and measurements of the charge collection efficiency. Central issues of the studies are the stability of the signal under electromagnetic irradiation and the linearity of the sensor response as a function of the number of particles crossing it in a time interval of a few ns. The results of the measurements are compared with results of the material analysis (Raman and photo-induced luminescence spectroscopy) performed by Fraunhofer IAF. The goal is to find wafer growth conditions to ensure very good and stable sensor quality.

In addition pCVD diamond sensors produced by Element Six^{TM} are studied to make a comparison of the sensor properties of different manufacturers.

The studied pCVD samples have a thickness of $300-900\,\mu$m and an area of $12\times12\,\mathrm{mm}^2$. On the substrate side of the sensors a few 10 up to 100μm are removed in order to improve the crystal quality and to reduce impurities. Both sides of a sensor have a three-layer Ti/Pt/Au metalization covering a $10\times10\,\mathrm{mm}^2$ area. On one side the metalization has a four pad structure.

In addition to the research activity at DESY, a research group is established in NC PHEP (Minsk) to make studies of diamond detectors. The main goal of their activity is to make cross-checks of the results with DESY and to study the effects of surface treatment on the detector properties of diamond [34].

7.1 Electrical Properties

Measurements of the current through a diamond sample as a function of the applied voltage are done as the first step of the studies. For most of the sensors the current has an almost linear dependence on the voltage and stays in the picoAmpere (pA)-range for an electric field up to about $2\,\mathrm{V}/\mu$m.

For several samples produced by Fraunhofer IAF a sharp current increase up to $1-100\,$nA is observed even for much lower strength of the electric field. In most cases the current measurements done for individual pads show localized areas to be responsible for the observed breakdowns. A visual inspection of the diamond surface revealed macroscopic defects (micro-cracks) as a possible reason for the high current. Figure 28 shows a micro-crack visible on the magnified view of the diamond surface near a metalization edge.

As it was noticed, the micro-crack density increases with the thickness of a diamond wafer. During the growth process a surface tension becomes stronger with the thickness of the deposited material and leads to the micro-crack formation. As a possible improvement of the diamond sensor quality a limitation of the wafer thickness to $500\,\mu$m will be considered in the future.

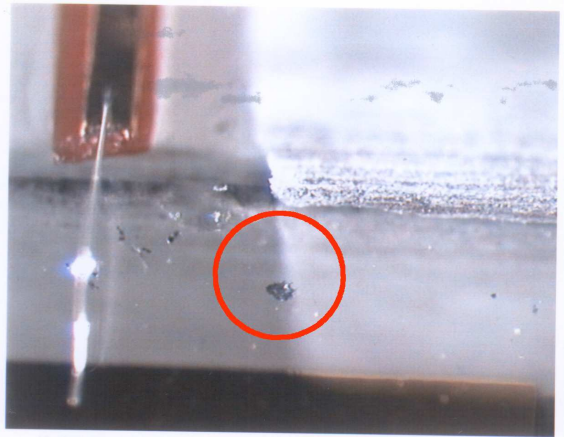

Figure 28: A magnified view of the diamond surface with a micro-crack observed near a metalization edge.

7.2 Charge Collection Efficiency

For the selected sensors with a low current the average charge induced by a minimum ionizing particle crossing the sensor bulk is measured as a function of the electric field strength. The charge collection efficiency is defined as the ratio between the measured charge and the total charge produced by the ionizing particle which is calculated from the energy deposition.

For each value of the voltage applied the charge collection efficiency is measured several times at intervals of 10 minutes in order to study the stabilization processes. For most of the measured polycrystalline samples the charge collection efficiency decreases with time down to a stable value. The samples exposed to irradiation with ^{90}Sr electrons up to about 100 Gy of the absorbed dose show a more pronounced time dependence of the charge collection efficiency in comparison with the results obtained before the irradiation.

Figure 29 shows the charge measured in different time intervals after the voltage was changed as a function of the applied electric field. The charge collection efficiency grows with the electric field strength. No saturation is seen up to this field strength.

A possible reasons for the long stabilization processes of about half an hour is maybe a non-uniform distribution of charge traps inside the diamond bulk. In the case of a low detrapping probability the number of trapped charge carriers increases with time up to an equilibrium value. If the traps are distributed non-uniformly, what is very likely for the polycrystalline material, the trapping of charge carriers leads to a formation of local space charges, which partly compensate the applied electric field and causes a decrease of the charge collection efficiency.

The measurements done for a single-crystal CVD diamond produced by Element Six shows no time dependence of the charge collection efficiency, as can be seen from Figure 30. The charge collection efficiency grows with the electric field strength and is saturated already at about 0.12 V/μm.

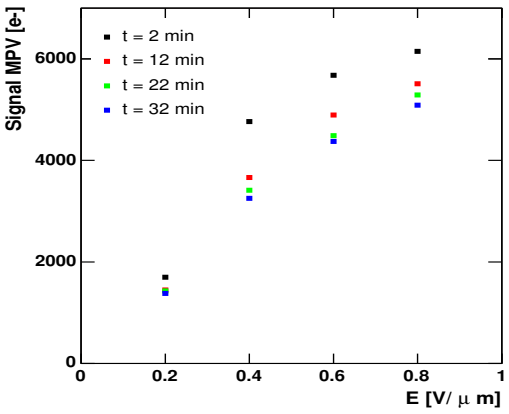

Figure 29: The signal of a Mip measured as a function of the applied electric field. The measurements are done 2, 12, 22 and 32 minutes after the field was applied. The signal is given as the number of electrons measured for the most probable value (MPV) of a Mip

7.3 Diamond Response as a Function of the Absorbed Dose

The charge collection efficiency is measured as a function of the absorbed dose. The irradiation is performed with a ^{90}Sr beta source up to about 100 Gy within a few days. The voltage applied to a sample corresponds to 1 V/μm of field strength. The charge collection efficiency and the current in the voltage supply circuit are monitored during the irradiation.

For some of the studied sensors produced by IAF a degradation of charge collection efficiency down to zero was observed already at about 1 Gy of the absorbed dose along with a dramatical current increase which results in a high noise level. This batch of samples showed also a high concentration of micro-cracks.

However, for most of the samples a fast stabilization of the charge collection efficiency occurs during the first few Gy of the absorbed dose. Figure 31 shows the charge collection efficiency as a function of the absorbed dose measured for two different sensors. In both cases the current stabilizes simultaneously with the charge collection efficiency and stays at the level of $10 - 30$ nA.

7.4 Linearity of the Diamond Response

Measurements of the linearity of the sensor response were done with a hadron beam of about 4 GeV at the CERN PS in the year 2004. The accelerator was operated in the fast extraction mode and delivered bunches of $10^3 - 10^7$ particles within 10 ns. The measurements of the integrated charge induced during the bunch crossing were done over a wide range of the number of particles inside a bunch.

During the measurements a shielded box with a diamond sample as well as a trigger box with the scintillator are aligned to the beam axis by means of an xy-table. The scintillator is read out with two photomultiplier tubes via wavelength-shifting fibers. A coincidence of the discriminated signals from the photo-multipliers produces the trigger signal.

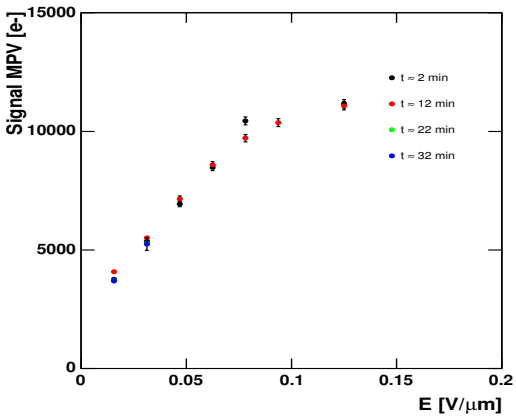

Figure 30: The signal of a Mip measured as a function of the applied electric field. The measurements are done 2, 12, 22 and 32 minutes after the field was applied.

The scintillator response was used also as a reference for the linearity measurements. Analog signals from both photo-multipliers were digitized with the ADC and gave a relative value of the particle fluence of the current bunch. The absolute values of the particle fluence measured by thermoluminescence dosimetry [35] for several intensities provided the calibration of the scintillator response.

Despite very low operating voltages, a nonlinearity of the photomultiplier response was observed in the high intensity runs. To correct the test-beam measurements for these nonlinearities the photomultiplier response was calibrated after the test-beam using an ultra-bright light emitting diode[36].

The response of two different diamond samples, one produced by Fraunhofer IAF and the other by Element Six, as functions of the particle fluence is shown in Figure 32. The fluence changes over nearly three orders of magnitude. The straight line represents a linear dependence and crosses also the signal size of a Mip. For the explored fluence range the deviation from linearity was found to be of at most 30%. This is comparable with the systematic uncertainty of the fluence calibration.

7.5 Alternative Technologies

Since large area CVD diamonds are relatively expensive we consider in addition also other radiation hard sensor materials;

- radiation hard planar silicon and
- planar GaAs.

Semi-insulating, undoped GaAs detectors have been shown to withstand doses up to 100 Mrad of 60Co gamma rays [37]. All three sensor materials will be investigated in parallel until a decision on the material is made. A mixed design is also possible. A first design of a sensor element with pads of less than one Moliere radius is planned to be manufactured as both a silicon and as a GaAs sensor as well.

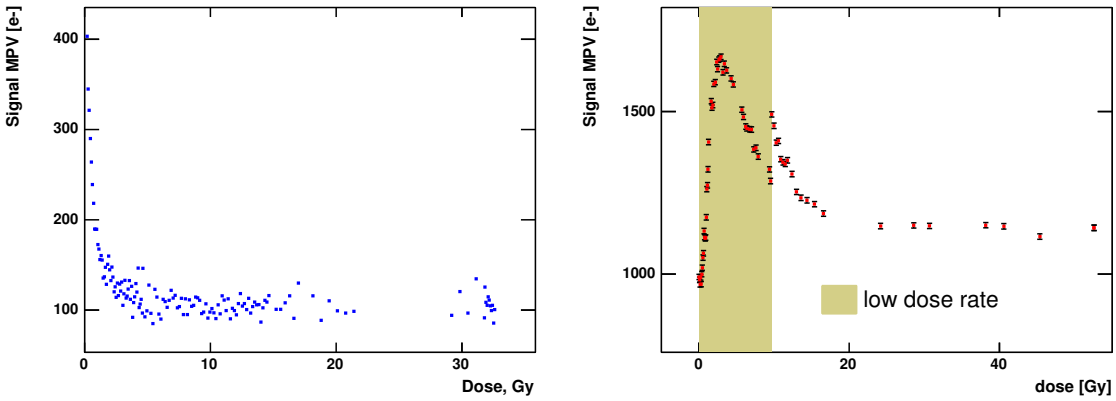

Figure 31: The charge collection efficiency as a function of the absorbed dose measured for two different samples produced by Fraunhofer IAF. The irradiation of the sample shown in the bottom plot was done with two different intensities. The low irradiation intensity during accumulation of the first 10 Gy corresponded to 0.15 Gy/h of the dose rate, the rest of measurements are done during irradiation with four times larger intensity.

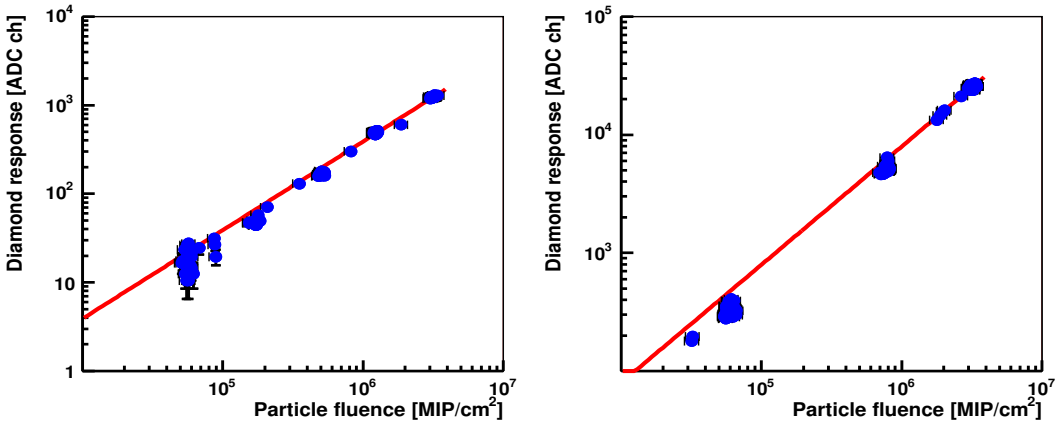

Figure 32: The response from diamond samples produced by Element6 (left) and FAP (right) as functions of the particle fluence.

8 Readout Electronics and Data Acquisition

For both calorimeters the readout electronics must provide for a full registration of all 3000 (6000 possible) bunches in a bunch train. Until the next bunch train the readout has to be completed and re-initialized. The dynamic range may last up to 1 : 10000. Additionally, the readout system of the BeamCal is foreseen to give direct feedback to the beam delivery system within a few microseconds. This 'fast' information may be restricted to a few sensor planes.

Currently different readout principles are being ered. The data can either be read out constantly with a 'streaming' system or it can be stored at the detector site until the bunch train's end. In this case it would be read out in between the bunch trains.

For each scheme a preamplifier including the analog chain until the ADC has to be designed. As a first step known readout systems are investigated and will be evaluated. In the current phase it is too early to decide on the final version of the readout design.

8.1 Readout Electronics for the LumiCal

From Monte Carlo simulations the amount of depositions on each sensor pad is known. To maintain the energy resolution of reconstructed showers from Bhabha events a dynamic range of about 1 : 1000 is required. Requiring in addition the detection of Mip particles, e.g. for alignment studies, the dynamic range must be extended to 1 : 20 000. Therefore a design using preamplifiers with switchable gain would be appropriate. Parallel shapers with different gains and switched output to the ADC could be used as well. They should have a peaking time of less than 100 ns to avoid pileup of signals. To digitize the signals a 10 bit ADC is connected to a group of channels. About 10 channels will be multiplexed to one ADC. A digital link, based on LVDS standard, will transmit the data to the DAQ. A scheme of the proposed solution is shown in Figure 33.

The LumiCal should also provide a raw luminosity measurement during data taking. Per bunch train we will have a few ten Bhabha events in the LumiCal, hence the differential luminosity can be determined in steps of several ten seconds. The mean occupancy in LumiCal is about 20% for a Bhabha event, so zero suppression will not be of large benefit. In addition there will be background from large area beamstrahlung remnants and two photon processes. Hence, very likely the whole LumiCal must be readout for each bunch crossing. The estimated amount of data per bunch train is about 1 Gbit. If digital data transmission from the calorimeter to the DAQ is done in the breaks between two bunch trains the necessary transmission speed is approx. 3 Gbit/s. Taking into account existing LVDS links with an available speed of 0.6 Gb/s, we would need only 5 digital links. For technical reasons (30 active layers of detector each divided to two half planes) 60 digital links will be foreseen. Space for electronics is foreseen at the outer radius of the calorimeter, as sketched in Figure 34.

The large number of readout channels favors the integration of the preamplifiers, shapers, multiplexers and ADCs with the detector. Heat dissipation and cooling parameters should be calculated carefully. Connection from each pad or strip to the readout electronics can be made using copper traces on a kapton flexfoil. Ultrasonic wire bonding between pad and

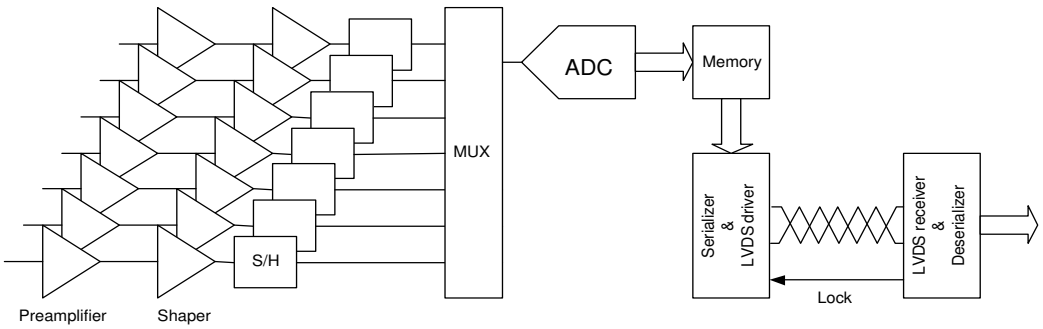

Figure 33: The proposed readout scheme for LumiCal using a multiplexed ADC.

readout traces can be made through a small hole in the flexfoil; bump bonding should be avoided, because of the larger technological risk and the higher price. To ensure minimal cross talk between signals in adjacent sensor pads or strips, additional grounded traces between signal lines are proposed. On one sensor half plane up to 720 channels of the readout electronics will be placed, thus requiring highly integrated chips. The use of a specialized readout chip with 64 or 128 channels each is planned. Technology options are radiation hard CMOS or bipolar manufacturing processes. The choice will be made in close collaboration with ECAL and HCAL groups. The first prototype of a preamplifier and shaper from Minsk University has been tested; the results are promising. The Minsk group is now working on an integration of 32 channels in one chip. A next step will the integration of the ADC.

8.2 Readout Electronics for the BeamCal

For the BeamCal the same type (compared to the LumiCal) of signal processing will be needed. Additionally a fast system for the direct feedback to the BDS is required. Such a system will process the data read out from the BeamCal on a dedicated DSP or FPGA farm with direct access to the first buffer stage. Information about the current luminosity can be fed directly into the feedback system FONT ([32]) after each bunch crossing. In addition, information on the beam parameters will be sent to the machine. The determination of the amount of information needed from the BeamCal is one of our next milestones. For this purpose a detailed Monte Carlo code based on GEANT4 is being developed.

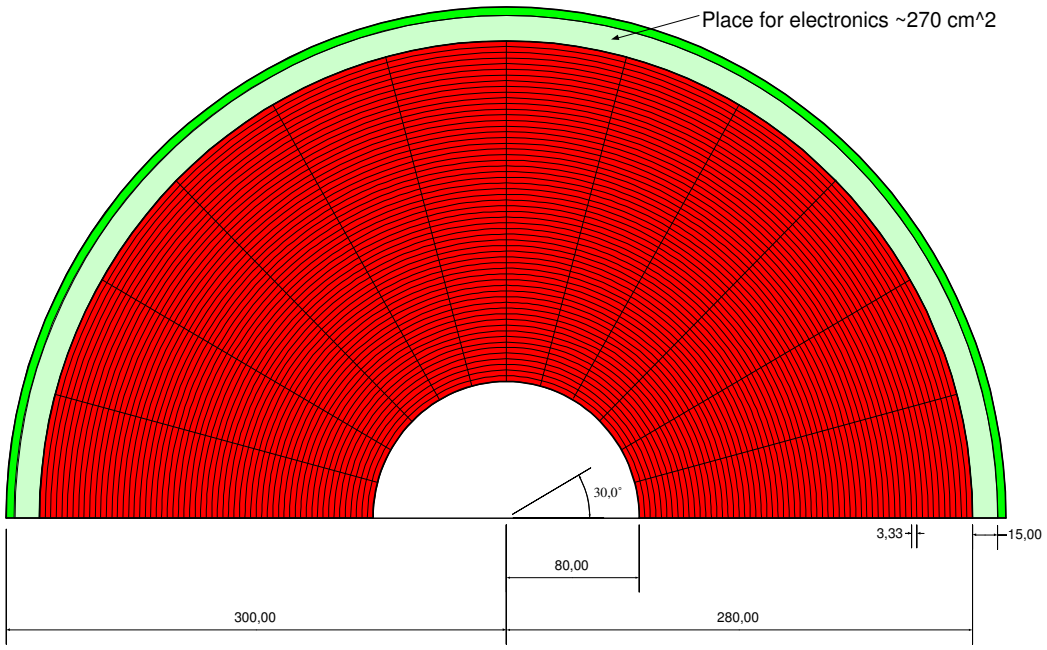

Figure 34: Half sensor plane for LumiCal with reserved space for electronic components at the outer radius.

9 The New Layout of the Forward Region

Over the last months the LDC [2] was revised. The goal was to minimize the detector costs but maintaining the performance. The detector is now shorter with some changes of the calorimeter end-caps. Also the instrumentation of the forward region was reconsidered. First, for the case of 20 mrad crossing angle the inner radius of LumiCal was enlarged, to avoid large depositions from beamstrahlung, as has been shown in Figure 15 of chapter 4.7. Also shown is the number of Bhabha events for a larger LumiCal inner radius per year. The statistics is still sufficient to match the precision requirement for the luminosity measurement. In parallel, also the polar angle coverage of BeamCal must be enlarged. In addition, the new design allows a smooth dismantling of the ILC detector and fast access to the tracking sub-detectors. The new geometry of the very forward region of the LDC [2] is shown in Figure 35 for 2 mrad beam crossing angle. Compared to earlier versions [4] other major changes are a new z-position, a larger outer radius of the LumiCal and an extension of the HCAL polar angle coverage adding LHCAL. The latter is also carried by the tungsten support tube and covers an angular range similar to the one of LumiCal. Between LumiCal and ECAL and also between HCAL and LHCAL space is left for cables and other infrastructure services for the inner detectors. This insensitive gaps are staggered, to ensure full coverage. The impact of the loss of ECAL performance over the gap between LumiCal and ECAL needs a careful investigation. For 20 mrad crossing

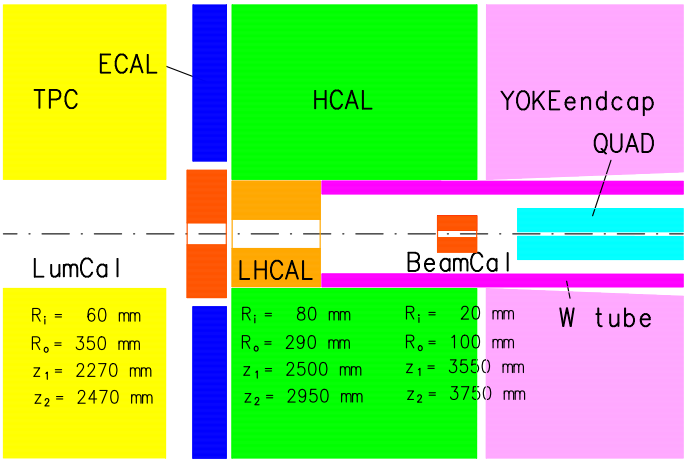

Figure 35: The very forward region of the Large Detector Concept as described in [2] for the 2 mrad beam crossing angle case. The IP is to the left. The tungsten tube supports the BeamCal and the LumiCal. Compared to earlier layouts LumiCal is now in front of the hadron calorimeter (HCAL). The distance of LumiCal to the IP has been significantly decreased to about 2.3 m. To keep an angular coverage over HCAL the outer radius of LumiCal has been increased to 350 mm. The BeamCal position and dimension is almost unchanged. Quad is the last quadrupole magnet of the BDS.

angle the design is shown in Figure 36. No simulation studies are done so for for this new

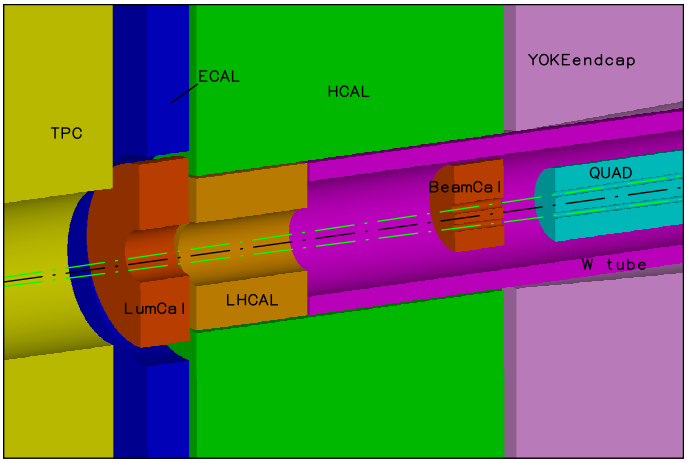

Figure 36: The very forward region of the Large Detector Concept as described in [2] for the 20 mrad beam crossing angle case. The IP is to the left. The tungsten tube supports the BeamCal and the LumiCal. The distances of the calorimeters from the IP are the same as in the previous Figure.

design. The performance studies presented in this report for BeamCal and LumiCal will hold also for the new design of the forward region. The different z-position of LumiCal may need a redesign of the pad and strip sizes on the sensor planes. Changes are expected for the background occupancy in the inner detector due to backscattering low energy particles. Also the background in the LumiCal may change for some versions of the magnetic field in the detector and a 20 mrad beam crossing angle. A detailed study will be done and is part of the milestones given.

10 Previous Milestones for LumiCal MC Simulations

The status of the milestones given in the previous report in October 2004 to the PRC are discussed in the following. Please take note that many of the milestones cover a period longer than one and a half year.

10.1 Previous Milestones for LumiCal MC Simulations

These milestones cover 2 - 3 years. The main focus was transitioning from a head-on collision design to a nonzero crossing angle and developing a high statistics and fast simulation to map the detector required performance and alignments needs. Although simulations of a more realistic calorimeter design including production constraints, sensors, digitization, electronics noise were performed, we intend to extend and deepen these studies further. The physics background study is not complete and requires study of additional processes. Both pad and strip designs fulfill the required precision, however the final decision will have to await more sophisticated background and sensors studies. Here we can conclude that all milestones are addressed.

10.2 Previous Milestones for Mechanics and Alignment

The milestones of mechanical design, alignment and sensors prototyping were partially addressed. Progress is made in particular with the development of the laser alignment system including 3D displacement probing capabilities. No progress is made in designing a more detailed mechanical structure with decoupled sensor planes and absorber disks.

10.3 Previous Milestones for Sensor Prototyping

These milestones cover 3 years.

Only first design steps towards sensor prototyping are done. More effort is needed in the next years.

10.4 Previous Milestones for BeamCal MC Simulations

The changes in the beam delivery system of the ILC have been thoroughly investigated as well as the impact of different beam parameter settings as they are under discussion for the ILC. It has been found that the electron reconstruction efficiency is sufficient for challenging particle searches like stau in SUSY scenarios. An investigation of the electron detection efficiency as a function of the granularity shows that a segmentation of about half a Molière radius leads to the highest reconstruction efficiency. A more rough segmentation, e.g. $0.8\,R_M$ deteriorates the performance slightly.

The simulation of the beam diagnostics capabilities has been significantly enhanced and the impact of the new detector layout and the BDS changes have been studied. A full Geant4 simulation for this purpose is under test at the moment. A sensor calibration using Bhabha events has not yet been investigated but will be done in the future if all necessary tools are available.

Since for these milestones a period of two or three years was foreseen we conclude that we are well prepared to match them.

10.5 Previous Milestones for BeamCal Sensor Prototyping

There are milestones about linearity and homogeneity measurements and material effects about which we promised results now.

The linearity of CVD diamond sensors has been tested for particle fluences between 2×10^4 and 6×10^6 particles per 10 ns. Taking into account the size of the signal for a Mip good linearity can be expected over 6 orders of magnitude. During the production of the sensors last year the failure mode of micro crack formation has been found, having delayed the studies on the sensor homogeneity and material features like annealing.

For the other milestones we promised results end of next year. The status is as follows: A large number of sensors has been built by the IAF and Raman and photoluminescence spectra have been used to define quality criteria for the material selection. We have just agreed with FAP to produce a batch of sensors with improved parameters.
For the investigations of irradiation up to highest doses we prepare at the moment a test-beam measurement in June 2006. The work on these milestones is ongoing.

Just now we are not prepared to propose a prototype calorimeter on the basis of diamond sensors. More experience in the controlled production of a larger amount of diamond sensors with comparable quality is necessary. As alternatives, we also study the behavior of silicon and GaAs sensors as a function of the absorbed dose of electromagnetic radiation up to MGy. Some essential items still to be solved before we can decide on a prototype are given in the new milestones for BeamCal.

We would like to mention that the milestones concerning BeamCal hardware strongly depend on the support by the DESY-lab in Zeuthen. This support was not sufficient in the last year, but we are optimistic that the situation will be improved in the future.

10.6 Previous Milestones for PhotoCal

An algorithm for the determination of beam parameters from the beamstrahlung photons using PhotoCal based on a neural network approach showed results which were already presented in the last PRC report. The correlation between PhotoCal and BeamCal information has not been investigated further so far but will be pursued from the BeamCal side.

11 Milestones for Future R & D

11.1 Milestones for LumiCal simulation

- Little time was devoted to understanding the energy response of the calorimeter. The study of energy calibration and energy resolution have presently the highest priority. The requirements and possible limitations may influence the selection algorithm for Bhabha scattering events. (Till end of 2006)
- Implementation of the LumiCal in the present layout of the LDC detector within GEANT4 will be carried out. (Till end of 2006)
- Detailed and realistic simulation of the sensor response and attached electronics will be performed. (2007)
- Background studies will be extended to include high cross section processes to assess detector occupancy. (2006-2007)
- Clustering of energy deposits in LumiCal will be introduced. (2007)
- Tracking planes in front of LumiCal will be investigated, in order to assess the background rejection and to study in situ alignment with prompt muons. (2007-2008)
- The design of a digital calorimeter will be pursued to verify whether it is a viable option. (2006-2007)
- Further studies of the non-zero crossing angle will be pursued, including the influence of various magnetic field options.(2007-2008),

11.2 Milestones for BeamCal Simulations and Design

- Completing the tools for a full simulation of the beam diagnostics algorithm using BeamCal and determining the minimal set of information necessary for the fast feedback to the BDS: 12/2006
- Estimate of the background due to beamstrahlung on the forward calorimeters backscattered in the central detector for the new layout of the forward region: 03/2007
- Concept and component parameter for the fast readout chain for part of the BeamCal to be used for the feedback: 2007
- Test of algorithms for the fast feedback: 2007

11.2.1 R/O Electronics and Sensors

- Study of the performance of one-channel preamplifier to be delivered by NC PHEP (Minsk) for test-beam measurements: 07/2006
- Definition of parameters for multichannel prototypes: 09/2006 - 2007
- Engineering design and manufacturing of multichannel r/o electronics for test beam purposes: 09/2007 -2008
- Adaption of the PHY preamplifier technology, design of a test board (within Eudet): 07/2006

- Study of the performance of PHY type chips: 2006
- Development of a technical design of a readout concept for BeamCal and LumiCal: 2007
- Study of the performance of different sensor materials (CVD diamond, silicon, GaAs) in an electron beam as a function of the absorbed dose up to a few MGy: first run 2006/2007, subsequent runs very likely.
- Design of ultra-flat (gap between absorber layers!) readout structures on a sensor mock-up, optimization of parameters like signal shape, crosstalk, electrical symmetry: 03/2006 - 2007
- Development of prototype sensors based on silicon and GaAs: 2006
- Manufacturing of prototype sensors based on silicon and GaAs: 2007
- Continuation of the studies of large area CVD diamond material with the goal to control the production process to ensure a sufficient good homogeneity (collaboration with IAF Freiburg):2008
- Setup a laboratory for testing silicon sensors at TAU (2006/2007)
- Contact local Israeli industry for silicon design and production for the forward region detectors. establishing working relations including testing local products and first engineering design of sensors (2006-2007).

12 General Situation of the Project

Within FCAL the first diploma (2) and Ph.D. (1) theses have been finished. New young people are joining the groups and will overtake and extend the research work in the future. The European groups are part of the EUDET project, supporting the improvement of the research infrastructure for ILC detector R&D. These participating labs made firm commitments, in addition to the support obtained from the EU, to support the FCAL project. In addition several NIS institutes got support from INTAS. Applications to national funding agencies are pending in Israel or just being prepared in Poland. Belarus is ready for 'in kind' contributions to the readout electronics. FCAL is since 2006 also recognized as an research project in JINR, Dubna, and supported by an BMBF-JINR agreement.

Within the last years we developed the collaboration with groups working on the integrated luminosity performance beam diagnostics (EUROTEV) of ILC. There are many topics of overlap, and we agreed to continue the common effort.

W. Morse from BNL, who is engaged in the design of the forward instrumentation of the SiD detector, had loose contacts to FCAL over the last months. We agreed to unite our efforts in future.

13 Executive Summary

Since the last PRC report from the year 2004 the research work of the Forward Calorimetry group (FCAL) has been significantly deepened and extended. We give a few examples in this report to sharpen the physics cases for which high performance forward calorimetry is crucial. The performance of two of the three sub-detectors in the very forward region, LumiCal and BeamCal, is investigated for the two interaction regions of the baseline design of the ILC with beam crossing angles of 2 mrad and 20 mrad. Detailed MC simulation were done to optimize the design of both detectors taking into account the new challenges. The feasibility of high precision luminosity measurement is shown, after including machine and physics backgrounds, positioning tolerances, sensor structures and electronics requirements. For the larger crossing angle changes of the forward region compared to the head-on case of the TESLA TDR are necessary. BeamCal and LumiCal must be centered around the outgoing beam-pipe. The BeamCal will have a non-instrumented area to leave space for the second beam-pipe. The inner diameter of LumiCal must be enlarged to avoid substantial depositions from beamstrahlung. New systematic effects of the luminosity measurement, caused by the beam polarization and the bunch charge, are identified. Studies on background from other physics processes are presented but need to be continued. Further detector simulations including optimized sensor segmentations (shower peak design), a more realistic sensor and readout performance show the feasibility of a high precision luminosity measurement under more realistic conditions. Requirements on the readout electronics are derived from simulations. First exercises with a laser based position monitoring system for LumiCal show that a precision of a few μm can be reached. As an alternative technology for LumiCal, a digital calorimeter, is just being studied.

BeamCal simulations have shown a strong impact of the crossing angle, of the detector magnetic field and of the accelerator parameter settings on the amount and the distribution of the depositions caused by beamstrahlung e^+e^- pairs. For a lattice of different settings of these three quantities we have shown that beam diagnostics seems to be feasible with good precision for any design. The performance to detect high energy electrons, however, is different. The latter quantity is of crucial importance for several new particle searches, e.g. sleptons predicted by super-symmetry. An optimization of the detector segmentation is done to reach the highest electron detection efficiency at small polar angles. Diamond sensors, one option to instrument the BeamCal, are studied in a testbeam and with electrons from source. Results are presented on their response as a function of low radiation doses, and on the linearity of the response for large particle fluences. However, large area diamond sensors are still extremely expensive. Hence we extended the scope of sensor studies. Silicon and GaAs sensors will be tested for their performance as a function of the absorbed electromagnetic dose.

Conceptional design ideas for the front-end and readout electronics are discussed. To obtain prototype readout IC's for testbeam applications we established close contacts with groups from CALICE within the EUDET framework.

We also strengthened the collaboration with groups working on the integrated luminosity performance beam diagnostics (EUROTEV). We are looking forward to unite our research effort with SiD colleagues working on the forward instrumentation in BNL.

14 Miscellaneous

Since the last PRC report, we had three collaboration meetings. The talks given there can be found under:
http://www-zeuthen.desy.de/lcdet/
http://alzt.tau.ac.il/ fcal/
http://xtzeus3.ifj.edu.pl/ galas/fcal/

In addition, the following talks were given on conferences since the last PRC report:

W. Lohmann ~	Very Forward Region Summary, Machine Detector Interface Workshop, SLAC, January 2005.
W. Lohmann ~	Electron Detection in the Very Forward Region, Machine Detector Interface Workshop, SLAC, January 2005.
K. Mönig ~	What Precision do we need on the Luminosity Measurement?, Machine Detector Interface Workshop, SLAC, January 2005.
Ch. Grah ~	CVD Diamond Sensors for the Beam Calorimeter of the ILC, Machine Detector Interface Workshop, SLAC, January 2005.
Ch. Grah ~	Diagnostics with Beamstrahlung Electrons and Photons, Machine Detector Interface Workshop, SLAC, January 2005.
R. Ingbir ~	Luminosity Measurements using Bhabhas, Machine Detector Interface Workshop, SLAC, January 2005.
W. Wierba ~	Design of a Forward Calorimeter with Silicon Sensors, Machine Detector Interface Workshop, SLAC, January 2005.
W. Lohmann ~	Calorimeters for Instrumentation of the Forward Region, Linear Collider Workshop, SLAC, March 2005.
W. Lohmann for V. Drugakov and A. Elagin ~	Low angle Bhabha events and Electron Veto - Comparison Between Different Crossing Angles, Linear Collider Workshop, SLAC, March 2005.
V. Drugakov, W. Lohmann and A. Stahl ~	Design and Performance of a Beam Calorimeter for an ILC Detector, DPG meeting, Berlin March 2005.
U. Nauenberg ~	Study of electronics requirements for good resolution and detector simulations, Linear Collider Workshop, SLAC, March 2005.
K. Kouznetsova ~	Calorimeter technologies for forward region instrumentation, Linear Collider Workshop, SLAC, March 2005.

R. Ingbir ~	Luminosity measurement, Linear Collider Workshop, SLAC, March 2005.
Ch. Grah ~	FLUM: Fast Luminosity Monitoring, ILC-European Regional Meeting and ILC-BDIR, RHUL London, June 2005.
W. Lohmann ~	IP Instrumentation, International Linear Collider Physics and Detector Workshop, Snowmass USA, August 2005.
W. Lohmann ~	Instrumentation of the Very Forward Region of a Linear Collider Detector, International Linear Collider Physics and Detector Workshop, Snowmass USA, August 2005.
V. Drugakov ~	Instrumentation of the Very Forward Region of a Linear Collider Detector, Summer School on "Actual Problems of Microworld Physics", Gomel, Belarus, August 2005.
H. Abramowicz ~	Luminosity Measurement Requirement, International Linear Collider Physics and Detector Workshop, Snowmass USA, August 2005.
H. Abramowicz ~	Luminosity Detector for the ILC, International Linear Collider Physics and Detector Workshop, Snowmass USA, August 2005.
W. Lohmann for H. Abramowicz ~	Luminosity Measurement, International Linear Collider Physics and Detector Workshop, Snowmass USA, August 2005.
A. Elagin ~	Optimized sensor segmentation for BEAMCAL, International Linear Collider Physics and Detector Workshop, Snowmass USA, August 2005.
P. Bambade ~	Comparing BEAMCAL eveto for 2 and 20 mrad, International Linear Collider Physics and Detector Workshop, Snowmass USA, August 2005.
I. Bozovic-Jelisavcic ~	Four-lepton neural current processes as background for luminosity measurement, ECFA-DESY Linear Collider Workshop, Vienna, November 2005.
B. Pawlik ~	LumiCAL Simulation, ECFA-DESY Linear Collider Workshop, Vienna, November 2005.
A. Sapronov ~	Systematic effects on luminosity measurement at 2 and 20 mrad beam crossing angles, ECFA-DESY Linear Collider Workshop, Vienna, November 2005.
R. Ingbir ~	The very forward region, ECFA-DESY Linear Collider Workshop, Vienna, November 2005.
R. Ingbir ~	Luminosity calorimeter - design recommendation, ECFA-DESY Linear Collider Workshop, Vienna, November 2005.

V. Drugakov ~	BeamCal Performance at different ILC designs, ECFA-DESY Linear Collider Workshop, Vienna, November 2005.
K. Afanaciev ~	Studies on large area diamond sensors, ECFA-DESY Linear Collider Workshop, Vienna, November 2005.
K. Afanaciev ~	Studies on large area diamond sensors, ECFA-DESY Linear Collider Workshop, Vienna, November 2005.
Ch. Grah ~	Analysis of Beamstrahlung Pairs for Luminosity, ECFA-DESY Linear Collider Workshop, Vienna, November 2005.
Ch. Grah ~	Fast and Precise Luminosity Measurement at the ILC, Linear Collider Workshop, Bangalore, March 2006.
W. Lohmann ~	Testbeam Plans for Forward Instrumentation, Linear Collider Workshop, Bangalore, March 2006.
C. Rimbault ~	Systematic limitations to luminosity determination in the LumiCal acceptance from beam-beam effects, Linear Collider Workshop, Bangalore, March 2006.
V. Drugakov ~	BeamCal Performance for Different ILC Detector Concepts, Linear Collider Workshop, Bangalore, March 2006.
W. Wierba ~	Very Forward Calorimeter readout and machine interface, Linear Collider Workshop, Bangalore, March 2006.
R. Ingbir ~	Simulations of the Forward Region, ILC Software Tools Meeting, Cambridge 2006.

References

[1] H. Abramowicz et al., *Instrumentation of the Very Forward Region of a Linear Collider Detector*, IEEE transactions of Nuclear Science, 51, p, 2983 2004

[2] LDC Working Group, *The LDC Outline Document*, in the current version of v1.3.

[3] *TESLA Technical Design Report*, DESY 2001-011, ECFA 2001-209, March 2001.

[4] A. Stahl and K. Büsser, *Detector Concept of the Forward Regions*, LC-DET-2004-034.

[5] S. Riemann, private communication.

[6] G. Altarelli et al., Phys. Lett. **B349** (1995) 145.

[7] R. Hawkings, K. Mönig, EPJdirect **C8** (1999) 1.

[8] M. Battaglia et al., Eur.Phys.J.C33:273-296 (2004)

[9] P. Bambade et al., *Experimental implications for a linear collider of the SUSY dark matter scenario*, talk given at International Conference on Linear Colliders (LCWS04), Paris France, April 2004.

[10] T. Raubenheimer et al., *Suggested ILC Beam Parameter Ranged*, available at http://www-project.slac.stanford.edu/ilc/acceldev/beamparameters.html.

[11] L. Hendrikson et al., *Luminosity Optimization Feedback in the SLC*, ICALEPCS Conf. (1997).

[12] A. Stahl, *Diagnostics of Colliding Bunches from Pair Production and Beam Strahlung at the IP*, LC-DET-2005-003.

[13] T. Tauchi and K. Yokoya, *Nanometer-beam-size measurement during collisions at linear colliders*, Phys. Rev. E 51, 6119-6126 (1995).

[14] B. Parker and A. Seryi, *Compensation of the effects of a detector solenoid on the vertical beam orbit in a linear collider*, Phys. Rev. ST Accel. Beams 8, 041001 (2005).

[15] G. Abbiendi et al., OPAL Collaboration, Precision luminosity for Z0 lineshape measurements with a silicon-tungsten calorimeter, 28th September 1999 CERN- EP/99-136, Eur. Phys. J. C14(2000)373-425.

[16] see e.g. M. Czakon, J. Gluza and T. Riemann, hep-ph/0604101, DESY 06-021, *submitted to Elsevier Science.*

[17] S. Jadach, talk given on the FCAL workshop, Cracow 2006, http://xtzeus3.ifj.edu.pl/ galas/fcal/index.html

[18] D. Schulte, Ph. D. Thesis, University of Hamburg 1996. TESLA-97-08.

[19] S.Jadach, W. Placzek, E. Richter-Was, B.F.L. Ward and Z.Was, BHLUMI, A Monte Carlo Event Generator for BhaBha Scattering at Small Angles, Version 4.04.

[20] A. Stahl, *Luminosity Measurement via Bhabha Scattering: Precision Requirements for the Luminosity Calorimeter.*, LC-DET-2005-004, Apr 2005.

[21] L. Suszycki, LumiCal background studies, talk given at FCAL Research Workshop of the Israel Science Foundation, Tel Aviv, Israel, 18-22 September, 2005.

[22] I. Bozovic-Jelisavcic, Four-lepton neural current processes as background for lumi nosity measurement, talk given at the 4th International Linear Collider Workshop 2005 ECFA Study, Vienna, Austria, 14-17 November, 2005.

[23] J.A.M Vermaseren , Nucl. Phys. B229(1983)347.

[24] W. Kilian, WHIZARD 1.40 A Generic Monte Carlo integration and event generation pa ckage for multi-particle processes (LC-tool 2002-039).

[25] B.Pawlik, BARBIE Version 4.1, Simulation package of the TESLA luminosity calorimeter, private communication.

[26] R. Ingbir, Luminosity detector design recommendation, talk given at the 4th International Linear Collider Workshop 2005 ECFA Study, Vienna, Austria, 14-17 November, 2005.

[27] W. Lohmann et al., *Instrumentation of the Very Forward region*, PRC R&D 02/01.

[28] R. Brun, F. Bruyant, M. Maire, A.C. McPherson, P. Zanarini, *GEANT3*, Preprint CERN DD/EE/84-1, 1984, revised September 1987.

[29] W. Placzek et al., Phys. Lett. **B390** 298, 1997.

[30] S. Agostinelli et al. [GEANT4 Collaboration], *GEANT4: A SIMULATION TOOLKIT*, Nucl. Instrum. Meth. A **506** (2003) 250.

[31] D. Karlen e al., Phys. Rev. **D39**, 1861, 1989.

[32] FONT: Feedback on nanosecond timescale, project homepage at: http://hepwww.ph.qmul.ac.uk/ white/FONT/

[33] G. White, *Multi-Bunch integrated ILC Simulations*, talk given at International Linear Collider Physics and Detector Workshop, Snowmass USA, August 2005.

[34] K.G. Afanaciev et al., *Characterization of Diamond Detectors*, International School-Seminar, The Actual Problems of Microworld Physics, Belarus, Gomel, 2005.

[35] D. Chong et al., *Validation of Synthetic Diamond for a Beam Condition Monitor for the Compact Muon Solenoid Experiment*, to be published.

[36] K. Kousnetzova, thesis, Humboldt University 2006, to be published.

[37] S.P. Beaumont et al., Nucl. Instr. and Meth. A322 (1992) 472-482.